Infective/inflammatory disorders

Poster No.:	A-887
Congress:	ECR 2017
Type:	Invited Speaker
Authors:	J. Desimpel[1], M. Posadzy[2], F. M. H. M. Vanhoenacker[3]; [1]Duffel-Antwerp/BE, [2]Pozna#/PL, [3]Antwerp/BE
Keywords:	Musculoskeletal bone, Musculoskeletal joint, Musculoskeletal soft tissue, MR, Ultrasound, Contrast agent-intravenous, Infection, Inflammation, Abscess
DOI:	10.1594/ecr2017/A-887

Learning objectives

1. To learn about the pathomechanisms involved in inflammatory and infections disorders.

2. To understand the imaging appearances and their differential diagnosis in the acute, subacute and chronic phases of infection.

3. To become familiar with the spectrum of imaging features of inflammatory disorders in the axial and peripheral skeleton.

Main

I Musculoskeletal infection

A. Bone infection (osteomyelitis)

· **Definition**

Osteomyelitis is defined as a primary bone marrow infection with potential surrounding soft tissue involvement.

· **General clinical presentation**

Clinical presentation may vary and is often nonspecific. Patients present with fever and general malaise in the acute phase. Local swelling, pain and reduced movement of the affected limb are other possible symptoms. A male/female ratio of 2 to 1 is reported. The site of origin is mostly long bones, especially femur and tibia. Laboratory findings show an increase of c-reactive protein (CRP) and erythrocyte sedimentation rate (ESR) in the majority whilst white blood count may be normal. Cultures are essential for accurate treatment.

· **Pathogenesis and classification**

The underlying etiology is mainly due to hematogenous spread of a micro-organism. In 95% of the cases S. aureus is the infective agent. Other potential routes of contamination are summarized in table 1 and consist of spread from a contiguous source of infection

(Fig. 1 on page 12) open fractures with direct implantation and/or presence of a foreign body **(Fig. 2 on page 14)** post-operative infection due to instrumentation **(Fig. 3 on page 14).** Chronic osteomyelitis is also associated with vascular insufficiency (e.g. due to underlying diabetes mellitus) leading to chronic wounds. This exhibit will mainly focus on hematogeneous spread of osteomyelitis. Three clinical stages (acute, subacute and chronic) will be distinguished, although in clinical practice there is some overlap between the different stages.

Table 1. Main routes of infectious spread

1. Hematogeneous
2. Spread from contiguous source
3. Direct implantation
4. Postoperative infection

Thorough knowledge of age related vascularization is crucial to understand the pathophysiology and imaging pattern of hematogenously spread osteomyelitis (**Fig. 4 on page 16 , Fig. 5 on page 18 , Fig. 6 on page 19**).

After closure of the growth plate: From 16 years on restoration of the transphyseal vascularization may cause potential epiphyseal spread of infection.

Although traditionally the growth plate has been considered a barrier for epiphyseal extension of the infectious focus in children **(Fig. 7 on page 21)** this is a theoretical plain concept based on plain films. This barrier may be relative on MRI imaging as MRI is more sensitive to demonstrate subtle marrow changes as an early sign of infectious spread **(Fig. 7 on page 21, Fig. 8 on page 21)**.

In rare scenario's, the infection spreads predominantly by the circulus articuli vasculosus of Hunter supplying the epiphysis **(Fig. 9 on page 23).** This may explain rare occurrence of epiphyseal childhood osteomyelitis.

· **Imaging Findings**

Imaging findings depend on the subtype of osteomyelitis and the age of the patient. Consecutive changes occurring in acute osteomyelitis are summarized in **Fig. 10 on page 23 , Fig. 11 on page 24 , Fig. 12 on page 25 , Fig. 13 on page 26 , Fig. 14 on page 28 , Fig. 15 on page 29**.

Plain radiography is not sensitive for assessment of the osseous extent of the lesion in the first ten days after onset of infection. Nonspecific soft tissue swelling may be seen. Bony changes such as periosteal thickening, loss of trabecular architecture, osteopenia and osteolytic destruction are seen at earliest after one week. However, plain radiography is useful as a baseline study for further follow-up and for differential diagnostic purpose.

Inhomogeneous osteosclerosis and sequestrum (necrotic bone) is characteristic for chronic osteomyelitis. In some cases, a layer of new periosteal bone or involucrum is formed around the necrotic bone **(Fig. 12 on page 25 , Fig. 13 on page 26 , Fig. 17 on page 30 , Fig. 21 on page 35 , Fig. 22 on page 37 , Fig. 23 on page 39 , Fig. 24 on page 41).**

Ultrasound allows easy comparison of both sides. It is an accurate and quick tool to detect subperiosteal spread particularly in children because of loose attachment of the periosteum. Visualization of periosteal elevation, fluid collections or abscesses are signs suggestive of osteomyelitis. US will detect these signs earlier than standard radiography and allows US-guided biopsy and/or aspiration **(Fig. 11 on page 24).**

CT has a very limited role in acute osteomyelitis except for assessment of a sequestrum in chronic osteomyelitis. In the latter scenario, it is more accurate than plain radiography and MRI. A sequestrum represents a segment of necrotic bone that is separated from the living bone by granulation tissue and bone resorption **(Fig. 22 on page 37).**

MRI is the modality of choice for early detection of *acute osteomyelitis*. Changes in bone marrow are detected within three to five days after disease onset on FS T2-WI. Osteomyelitis can spread to the joint depending on the position of the joint capsule compared to the growth plate. An extra-articular growth plate does not predispose to joint infection, whereas intra-articular position of the growth plate may cause rapid spread to the adjacent joint **(Fig. 14 on page 28)** Soft tissue extension, joint effusion, abscess formation and sinus tracts are accurately visualized. A pathognomonic sign for acute osteomyelitis is the presence of fat globules on T1-WI. Islands of fat are released by necrotic lipocytes resulting in high signal intensity on T1-WI **(Fig. 16 on page 29)**.

Subacute osteomyelitis is characterized by the presence of a Brodie abscess **(Fig. 18 , Fig. 19 on page 33, Fig. 20 on page 33)** at the metaphysis not exceeding the growth plate in most cases. The shape of a Brodie abscess along the longitudinal

axis may be explained by effect of gravity. The penumbra sign consists of a subtle peripheral rim of high signal on T1-WI around the pus collection in the bone. The high SI is probably due to granulation tissue in the abscess wall with lipid-laden macrophages **(Fig. 18 on page 32)** After administration of intravenous gadolinium contrast, this thin vascularized rim enhances. (8,9)

Sequestrum formation is diagnostic for *chronic osteomyelitis*. Due to necrosis sequestrum is hypo-intense on all pulse sequences. Gadolinium contrast administration may reveal a cloaca (opening in the involucrum) through which pus, granulation tissue and sequestra can be discharged. In addition, enhancement of sinus tracts tracking from the bone to the skin surface is well demonstrated on contrast enhanced MRI **(Fig. 22 on page 37 , Fig. 23 on page 39 , Fig. 24 on page 41).**

Bone scintigraphy is able to detect osteomyelitis with high sensitivity. The specificity is -however- low. Multiplicity (e.g. in case of CRMO) is easily detected by this method.

Imaging features of acute osteomyelitis are illustrated on **Fig. 10 on page 23**, **Fig. 11 on page 24**, **Fig. 12 on page 25**, **Fig. 13 on page 26**, **Fig. 14 on page 28** , **Fig. 15 on page 29** , **Fig. 16 on page 29**.

Imaging features of subacute osteomyelitis are illustrated on **Fig. 17 on page 30**, **Fig. 18 on page 32 , Fig. 19 on page 33 , Fig. 20 on page 33**.

Imaging features of chronic osteomyelitis are illustrated on **Fig. 21 , Fig. 22 on page 37 , Fig. 23 on page 39 , Fig. 24 on page 41**.

· **Special subtypes of osteomyelitis**

Ø **Chronic Recurrent Multifocal Osteomyelitis (CRMO)**

Definition and pathogenesis

CRMO is defined as an auto-immune disease with recurrent inflammatory lesions of the bone. It typically affects children while the adult counterpart of the disease is known as SAPHO syndrome.

Imaging

Plain radiography initially shows an osteolytic lesion sometimes associated with periosteal reaction having a so-called "onion ring" appearance **(Fig. 25 on page 41)**. In later stages, there is progressive sclerosis of the bone.

MRI imaging shows bone marrow edema in active lesions with a hypo-intense signal on T1-WI and hyperintense SI on T2-WI **(Fig. 26 on page 42).** Transphyseal invasion may be visualized. Progressive sclerosis results in hypo-intense signal on both T1- and T2-WI and may be seen in subacute and chronic lesions. (10)

Ø **SAPHO**

Definition and pathogenesis

The combination of Synovitis, Acne, Pustulosis, Hyperostosis and Osteitis is defined as SAPHO syndrome. The underlying etiology is unknown. Osteitis is a key symptom with predominant involvement of the sternoclavicular joints and spine. Sacro-iliac joints are less commonly involved (Table 2).

Imaging

The affected joints show narrowing of the joint space on **plain radiography** with sclerosis and erosions of the joint facets in keeping with arthritis. Hyperostosis and enthesopathy are visualized.

CT is able to detect these bony changes more precisely.

MRI imaging is the preferred imaging technique for early detection. Bone marrow edema is visualized on FS T2-WI allowing to distinct acute and chronic lesions.

Fig. 27 on page 43 shows a typical bullhead sign of the sternoclavicular joint in SAPHO on CT and bone scintigraphy.

Fig. 28 on page 44 illustrates SAPHO of the spine.

According to other authors CRMO and SAPHO belong to the spectrum of spondylarthropathy rather than being an infection.

Table 2. Cardinal features of SAPHO

SAPHO: Synovitis - Acne - Pustulosis - Hyperostosis - Osteitis.

· Inflammatory disorder of unkown etiology.

· Involves preferentially axial skeleton (Sternoclavicular Joints - Spine - Sacroiliac Joints).

· Other locations may be involved as well (metaphyses!).

· Bone inflammation and reactive sclerosis and enthesopathy.

· DDx: Sclerotic metastasis, Lymphoma, Paget's disease.

Key points osteomyelitis

· Standard radiography is still the mainstay as a baseline examination and for follow-up and for differential diagnosis. A disadvantage is the latency time for detection of osseous involvement.

· Ultrasound is the preferred modality in case of suspicion of acute osteomyelitis in children or concomitant septic arthritis. US-guided biopsies and/or aspiration are safely and easily performed.

· The role of CT is very limited except for assessment of a sequestrum in chronic osteomyelitis.

· MRI is the preferred modality for early detection of osteomyelitis. The fat globule sign on T1-WI is pathognomonic for acute osteomyelitis whilst the penumbra sign is pathognomonic for a Brodie abscess in subacute osteomyelitis. A combination of T1- and FS T2-WI and gadolinium enhanced imaging is mandatory.

B. Infectious arthritis

· **Definition and pathogenesis**

Infectious or septic arthritis is defined as a destructive arthropathy caused by an intra-articular infection. S. aureus is the most frequent underlying micro-organism.

· **Imaging**

Standard imaging shows no abnormality in the early stages, except for peri-articular osteopenia. Narrowing of the joints with destruction of the subchondral bone are characteristic in late diagnosis.

Joint effusion is readily visualized on **ultrasound** with increased Doppler signal in case of disease activity. These findings are -unfortunately- nonspecific and may be seen in inflammatory arthritis or even in "toxic (transient) synovitis in children. Whenever infection is suspected, US guided aspiration of joint fluid is mandatory allowing culture of the aspirated fluid.

MRI imaging is the preferred technique for early diagnosis of bone marrow edema in active lesions (**Fig. 29 on page 46**).

C. Soft tissue infection

· **Pathogenesis and location**

The routes of infectious spread may be similar to the pathogenesis of osteomyelitis.

According to the involved soft tissue compartment, different groups of soft tissue infections may be distinguished (Table 3)

Table 3. Soft tissue infection according to the location of the lesion.

Location	Disease
Skin	Cellulitis
Fascia	Fasciitis
Muscles	Myositis / Abscess

Lymph nodes	Lymphadenitis due to Cat Scratch Disease
Bursae	Bursitis
Tendon	Tenosynovitis

· **Imaging**

Ultrasound of *cellulitis* reveals diffuse thickening of the skin and subcutaneous tissue. A pathognomonic cobble stone pattern appearance is explained by progressive fluid accumulation subcutaneously (**Fig. 30 on page 46 a**). MRI shows subcutaneous thickening with fluid collections with enhancement of the subcutaneous tissue and/or superficial fascia after gadolinium contrast administration (**Fig. 30 on page 46 b**). (12,13,14)

Standard imaging has a limited role in the diagnosis of *fasciitis* except in case of the characteristic presence of gas in the soft tissue. In early phases ultrasound imaging is more useful showing thickening of the fascia with adjacent subcutaneous edema. Subcutaneous edema is best visualized on T2-WI MRI images. Additionally subcutaneous emphysema may be present on CT. (13,14)

Focal myositis shows an enlargement and decreased signal intensity of the affected muscle on CT. MRI is the modality of choice to visualize the precise extension of myositis. Diffuse high signal intensity edema is seen on T2-WI. In contradistinction to most soft tissue tumors (except for a lymphoma), there is absence of disruption of the muscle bundles. The lesion may be complicated by abscess formation. (13,15)

An *abscess* characteristically shows a anechoic fluid collection on ultrasound in which septa may be present (**Fig. 31 on page 47 a**). The vascularized capsule is well evaluated by power Doppler. On CT-imaging a central necrotic component is surrounded by an enhancing vascularized capsular ring (**Fig. 31 on page 47 b**). Surrounding inflammatory stranding may be seen. In case of anaerobic infection, gas may be easily demonstrated on CT (**Fig. 32 on page 48)** or as dirty shadowing on ultrasound.(16)

Unilateral lymphadenopathy with marked intranodal and perinodal vascularization at certain locations such as the medial aspect of the elbow, the groin and to a lesser degree the popliteal fossa should raise suspicion of *cat scratch disease*. The patient should be inspected for any skin scratches and thorough anamnesis on contact with cats is required. Ultrasound shows a hypoechoic enlargement of the involved lymph nodes with central and perilesional hyperemia (**Fig. 33 on page 49)** An adjacent fluid collection may be

present. MRI reveals enlarged and enhancing lymph nodes. Serology may be needed to confirm *cat scratch disease.*(17,18,19)

Bursitis has a characteristic clinical presentation and rarely needs imaging for diagnosis. Fluid collection in the bursa is seen as an anechoic collection on ultrasound imaging. The lesion is of high signal intensity on T2-WI. After contrast administration enhancement of the bursal wall may be seen. The cause of bursitis is usually due to trauma, repetitive friction (**Fig. 34 on page 49**) or inflammation. Infectious bursitis is more rare. (13,20)

Imaging findings of *tenosynovitis* include an increase of fluid within the tendon sheath. Synovial thickening is suggestive of chronic pathology. Increased vascularity may be present on power Doppler images (**Fig. 35 on page 50**).(13)

II Musculoskeletal inflammation

This exhibit will mainly focus on the imaging features of peripheral manifestations of rheumatoid arthritis and axial manifestations of Spondylarthropathy (SpA).

A. Rheumatoid arthritis

· Definition and pathogenesis

Rheumatoid arthritis is a chronic progressive inflammatory disease characterized by polyarthritis. Patients present with an inflammatory type of pain and pathognomonic morning stiffness. The underlying etiology is unclear but genetic predisposition, environmental factors and auto-immunity are proven risk factors. An inflammatory response is triggered by the CD4 cells leading to pannus formation. It consists of edematous thickened synovium ("pannus") gradually eroding the articular cartilage causing fibrous ankylosis in late stage disease. Involvement of joint capsule, supporting ligaments, tendon (sheaths) and other soft tissues may occur as well.

· Imaging

Plain radiography may visualize structural abnormalities but these are often delayed findings. Although less sensitive than US and MRI, plain films remains useful as baseline examination for follow-up, for quick overview of different joints and to exclude other underlying causes of joint destruction including (erosive) osteoarthritis, gout or pseudogout. Juxta-articular osteoporosis and soft tissue swelling are early findings of RA. Progressive cartilage loss will lead to global narrowing of the joint space, whereas

degenerative osteoarthritis shows typically focal cartilage loss. The presence of bone erosions indicate intermediate stage (**Fig. 36 on page 51 , Fig. 37 on page 53**). In the end stage (sub)luxations and/or deformaty will be seen (**Fig. 38 on page 55**).

Ultrasound allows early detection and grading of the synovial inflammation or pannus with an increased signal on power Doppler, correlating with disease activity. An increase of (noncompressible) joint fluid is seen. Subtle bone erosions are better seen on ultrasound than on plain radiography (**Fig. 39 on page 55, Fig. 40 on page 56**). Rarely soft tissue involvement with formation of rheumatoid nodules are seen. Joints and tenosynovium are predominantly affected.

Early and subtle features of RA are detected on **MRI**. Bone marrow edema (BME) is seen in early disease stages and has a prognostic significance in predicting the development of erosions (**Fig. 41 on page 57**). Monitoring of disease activity is done by assessment of gadolinium contrast enhancement in active disease. The absence of global overview and limited access are important disadvantages of this technique. (22,23)

B. Axial Spondylarthropathy

· Definition and pathogenesis

Axial spondylarthropathy (SpA) consists of a group of different spondylarthritis involving predominantly the axial skeleton and sacroiliac joints (SIJ). Peripheral manifestation are dominated by enthesopathy rather than joint involvement. HLA-B27 gene positivity is highly associated. Other clinical characteristics are often needed for further subdivision of the different etiology (i.e. ankylosing spondylitis, psoriatic arthropathy, reactive arthritis, enteropathic SpA, SAPHO, …). Further discussion of these different clinical disease entities is beyond the scope of this exhibit, which will focus on cardinal imaging features.

· Imaging

A global overview of the structural abnormalities (erosion, sclerosis and later ankylosis) is visualized on **plain radiography (Fig. 42 on page 59, Fig. 43 on page 59, Fig. 45 on page 63)** also allowing differential diagnosis. Simultaneous occurrence of erosions, sclerosis and bony bridging in the SIJ is known as "variegated" sacroiliitis. A definite disadvantage is the fact that structural changes are relatively late findings. As a consequence, plain imaging plays no role in early detection of active inflammation.

Ultrasound has a limited role in the evaluation of SpA except for evaluation of pelvic or appendicular enthesopathy.

MRI allows early detection of bone marrow edema and disease activity (by gadolinium enhancement in active disease) (**Fig. 44 on page 61**). The ASAS criteria to diagnose sacroiliitis on MRI require BME in a typical juxta-articular subchondral location, either in the iliac or sacral bone. BME should be present in at least two areas or in one area on two consequent slices (27,28). It is the preferred modality for disease monitoring and detecting (neurological) complications (cauda equina syndrome, fracture dislocation with spinal cord injury in patients with spinal ankylosis). Disadvantages include limited access (long waiting lists) and difficulties in positioning of patients with anyklosis and gibbus. (24,25,26)

Key points inflammation

· Standard radiography is still useful for a global overview and for differential diagnosis. The main drawback is that it only shows delayed structural abnormalities caused by inflammation.

· Ultrasound allows early detection of peripheral arthritis. An increased signal on Power Doppler correlates with disease activity.

· MRI is the preferred modality for early detection of SpA revealing bone marrow edema in active lesions. The role of gadolinium contrast administration is still debated.

Images for this section:

Fig. 1: Infectious spread from contiguous infected tailors bunion. Axial T1-weighted image (WI) with FS after gadolinium administration shows an inflammed bunion with adjacent enhancement of the distal aspect metatarsal 5.

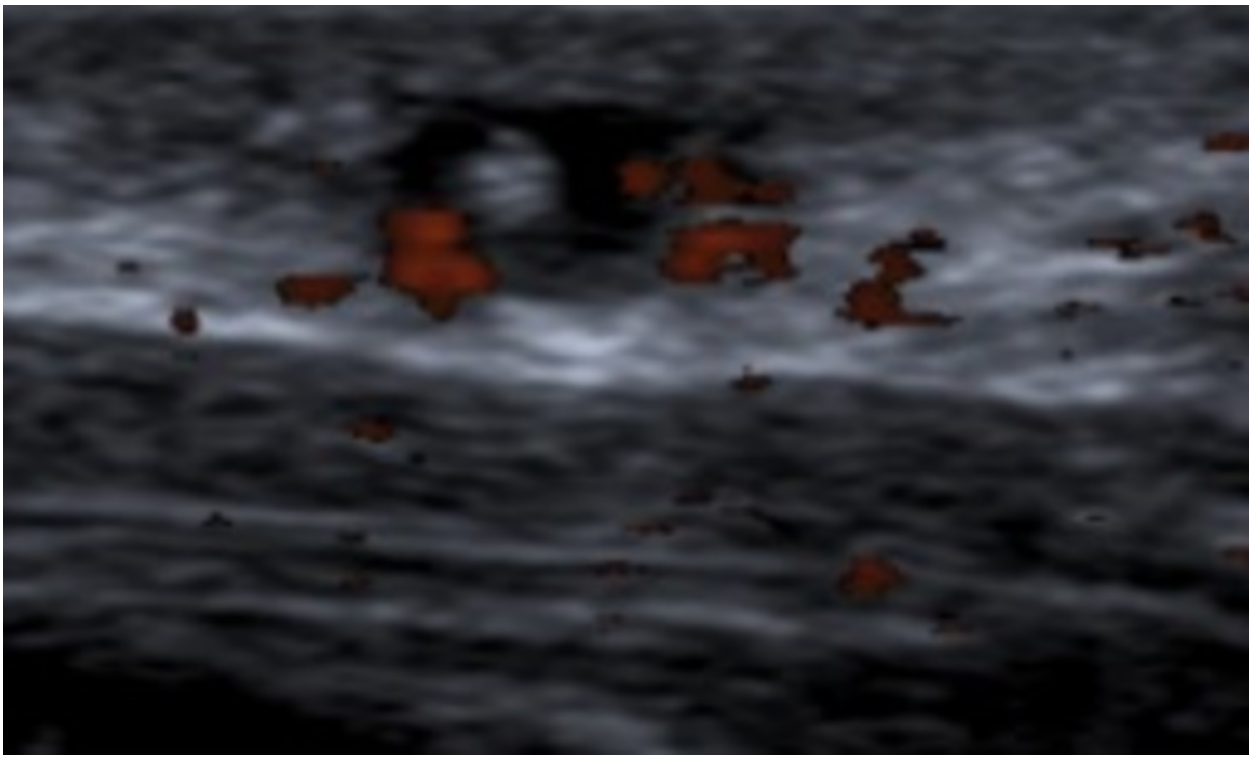

Fig. 2: Infection from direct implantation. Corpus alienum (wooden splinter) in the thumb area on ultrasound. Note small focal hyperreflection and surrounding hypo-echogenic halo with increased local vascularity seen on Power Doppler imaging.

Fig. 3: Postoperative infectious spread. Postoperative infection of the spine on sagittal T2-WI with FS after gadolinium contrast administration. Note postoperative status after laminectomy L4 and L5 with placement of intervertebral cages. Extensive enhancement of L5 and S1 with rim enhancement of the intervertebral cage L5-S1 in keeping with postoperative spondylodiscitis.

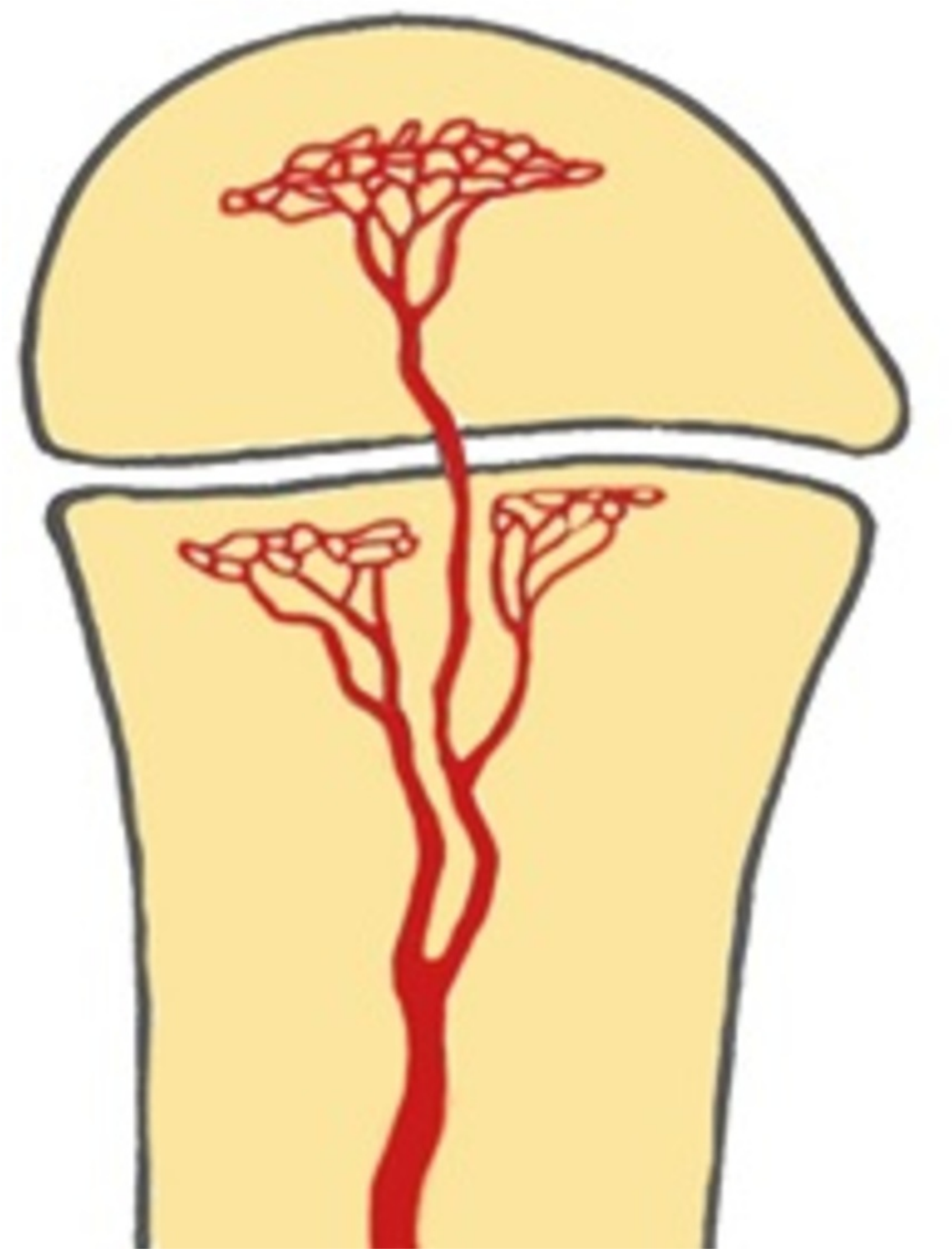

Fig. 4: Schematic drawing of vascularization of the long bone in infants. <18months: There are metaphyseal and transphyseal blood vessels allowing metaphyseal and epiphyseal origin of infection.

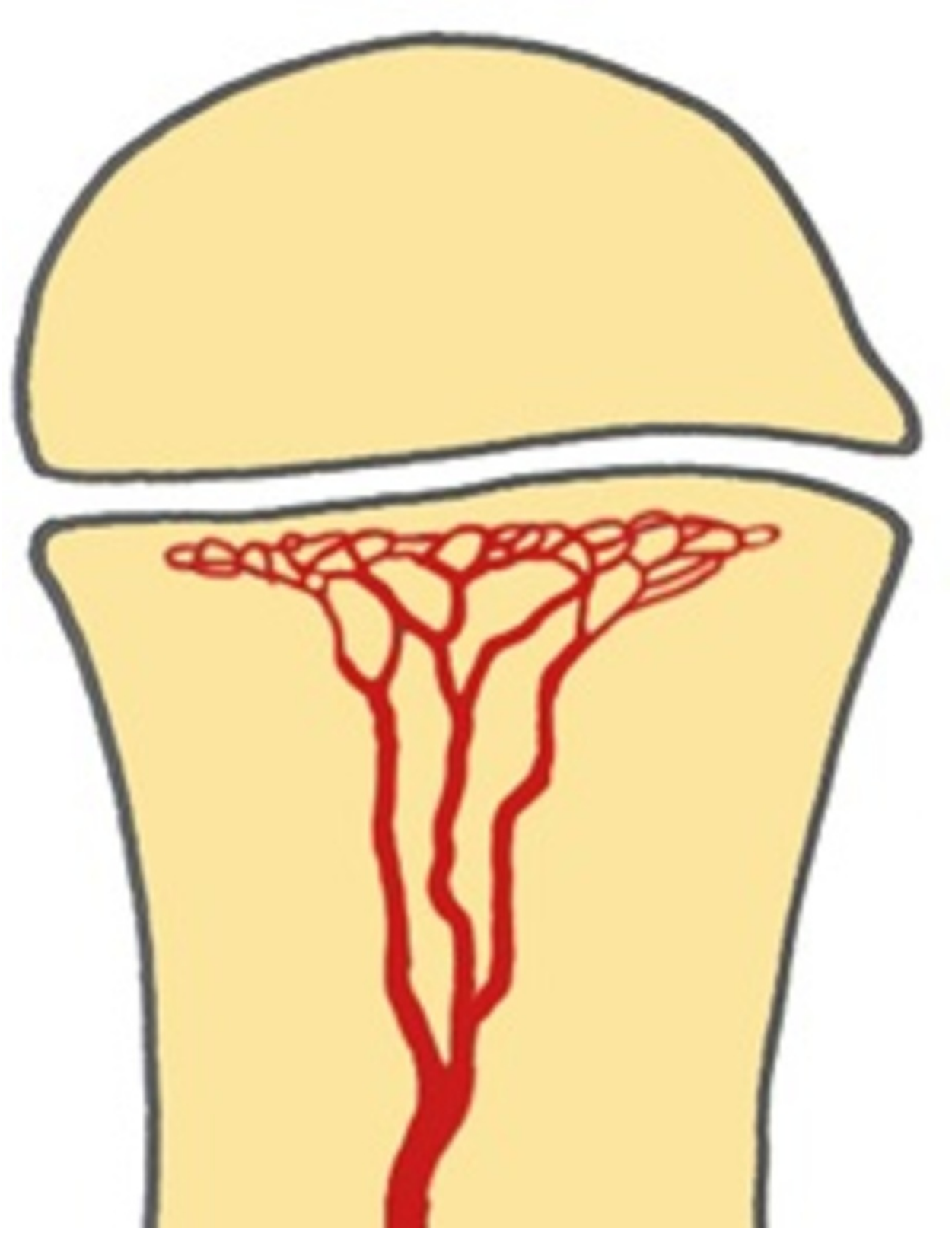

Fig. 5: Schematic drawing of vascularization of the long bone in children. 1-16 years: The epiphysis has its own nutrient vessels (veins and arteries) whilst the metaphysis and diaphysis share the same vessels. A natural barrier is formed by the physis preventing spread of osteomyelitis in the epiphysis and joints. Therefore, children of this age group will present with an initial and predominant metaphyseal focus of infection.

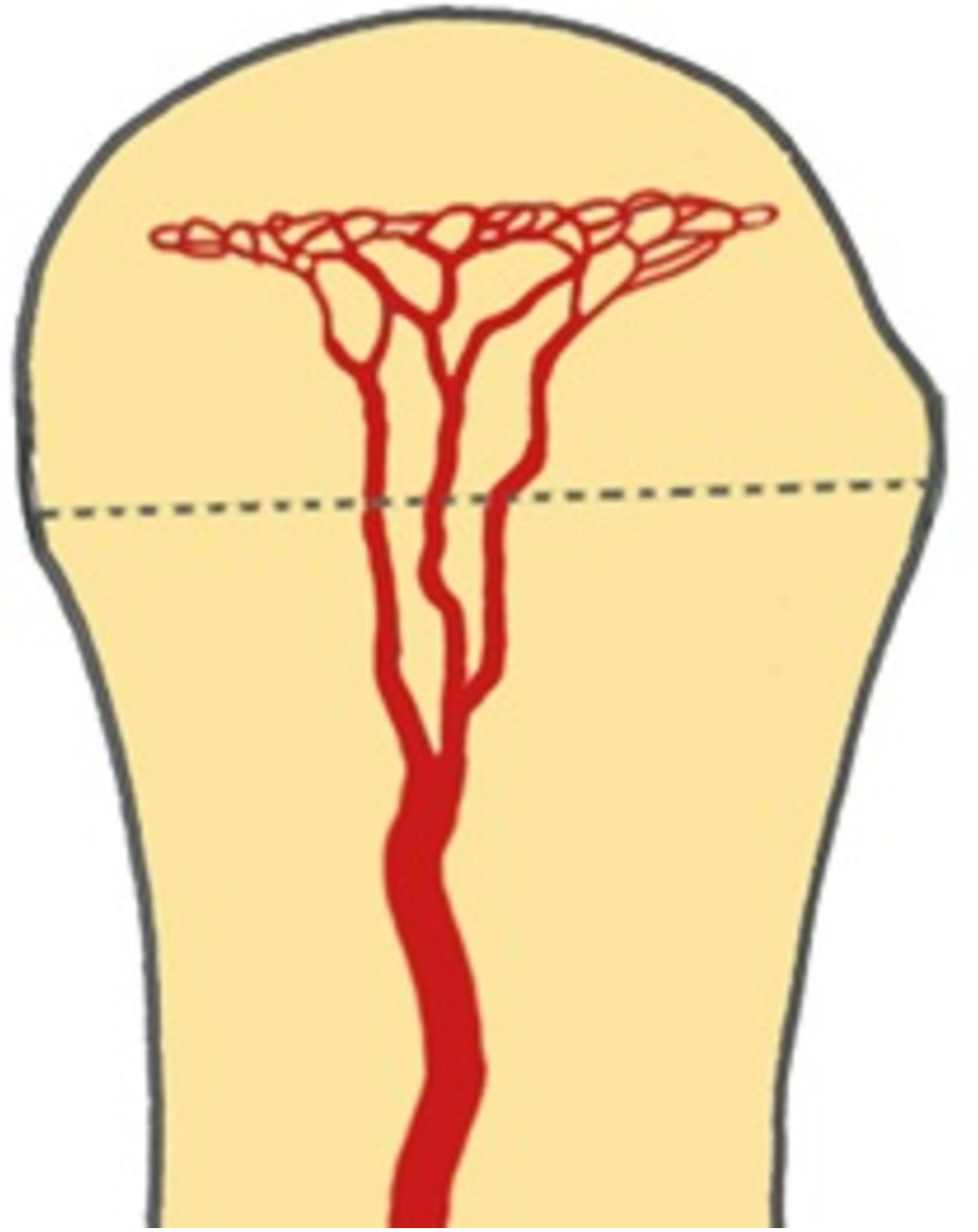

Fig. 6: Schematic drawing of vascularization of the long bone in adults. After closure of the growth plate: From 16 years on restoration of the transphyseal vascularization may cause potential epiphyseal spread of infection.

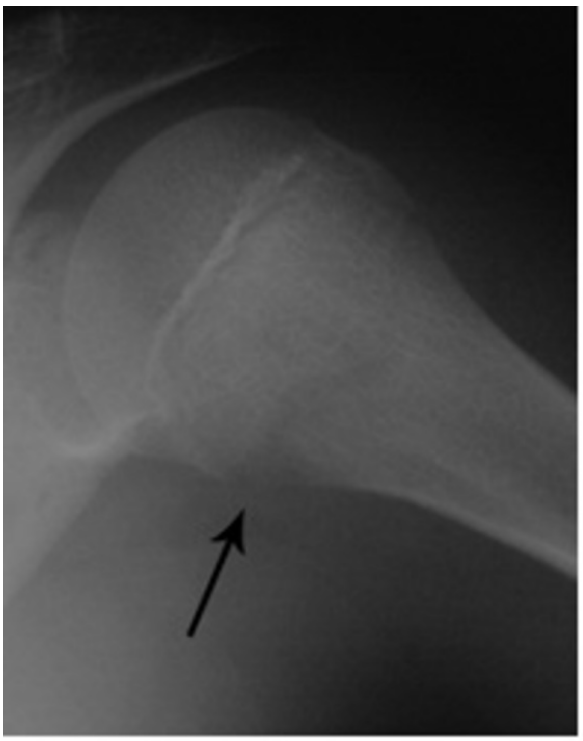

Fig. 7 a

Fig. 7 b

Fig. 7: Typical example of acute osteomyelitis of the left proximal humerus in a child with metaphyseal spread of infection. Plain radiography (Fig. 7 a) and coronal T2 weighted imaging (Fig. 7 b). Standard radiography shows a subtle osteolytic lesion at the metaphysis and loss of cortical lining of the medial humerus (black arrow). The surrounding bone marrow edema (black arrows) is limited to the metaphysis.

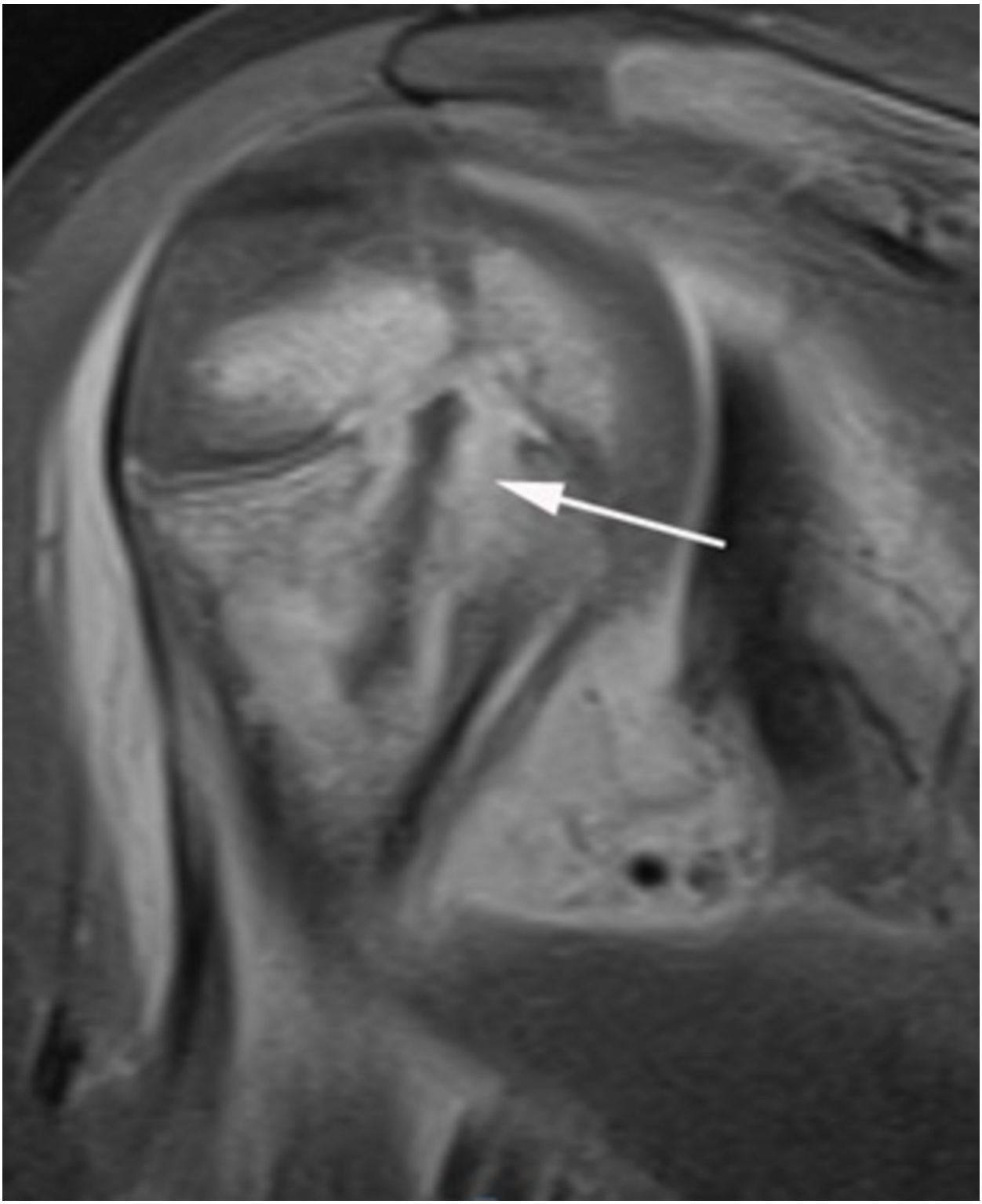

Fig. 8: Relative barrier of the growth plate on MRI. Another child with osteomyelitis in the right proximal humerus. Coronal T1-WI with FS after gadolinium contrast administration. The infection (white arrow) is mainly located at the metaphysis but there is at least some extension within the bone marrow into the epiphysis, in keeping with metaphyseal crossing.

Fig. 9 a

Fig. 9 b

Fig. 9: Epiphyseal childhood osteomyelitis of the right knee. Plain radiography (Fig. 9 a) and coronal T1-WI with FS after gadolinium contrast administration. Note focal hyperlucency (white arrow) in the epiphysis of the distal femur. After contrast administration (Fig. 9 b) the central part of the lesion is nonenhancing whereas a subtle peripheral rim enhances (white arrow) with surrounding enhancing bone marrow edema (black asterisk).

© F.M. Vanhoenacker, Department of Radiology, AZ Sint-Maarten, Duffel-Mechelen, Belgium

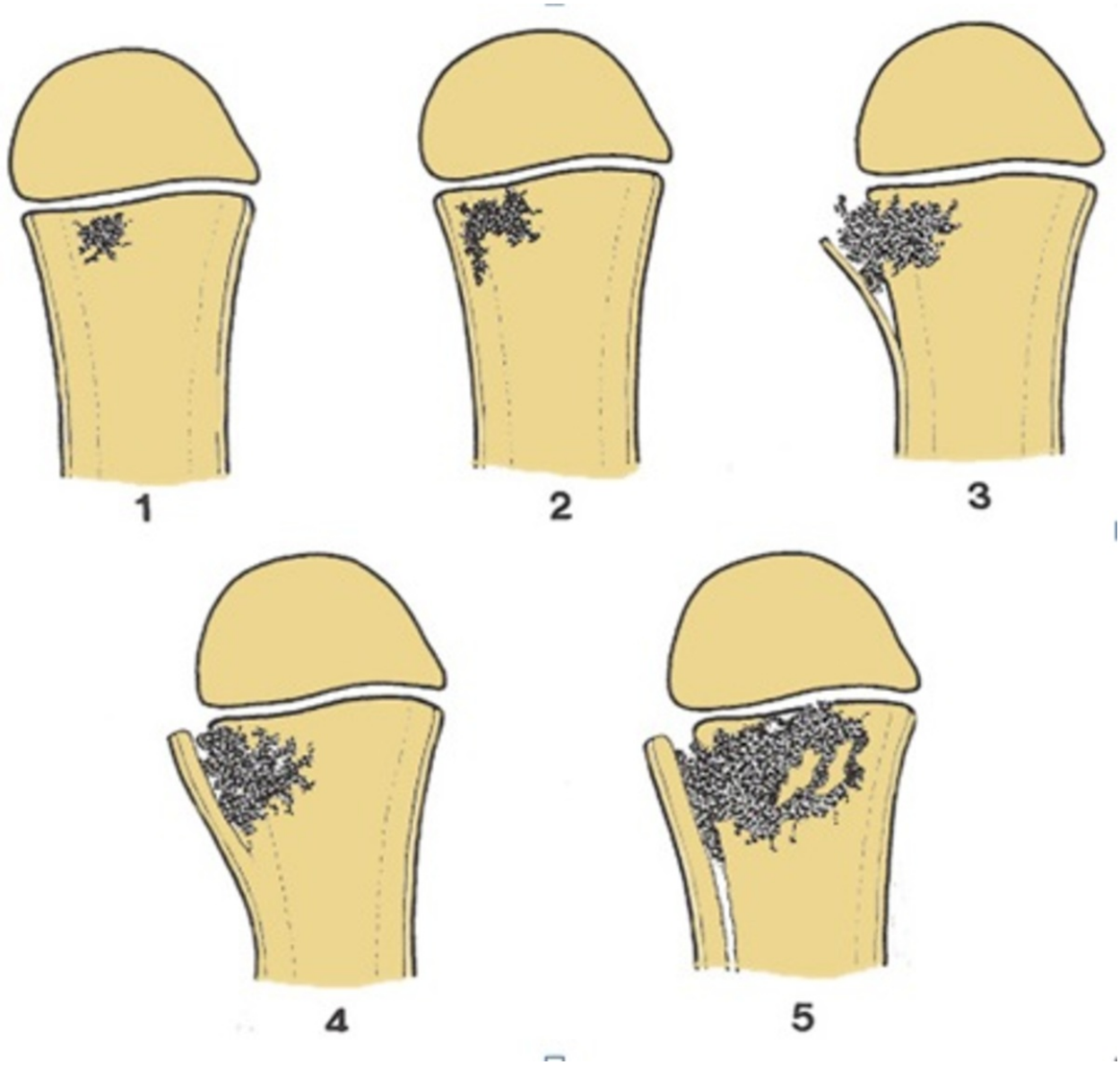

Fig. 10: Schematic drawing of the consecutive events of acute osteomyelitis. 1. Initial metaphyseal focus 2. Lateral spread to the cortex 3. Cortical penetration and periosteal elevation. 4. Formation of thick involucrum 5. Further expansion metaphyseal focus with reactive involucrum.

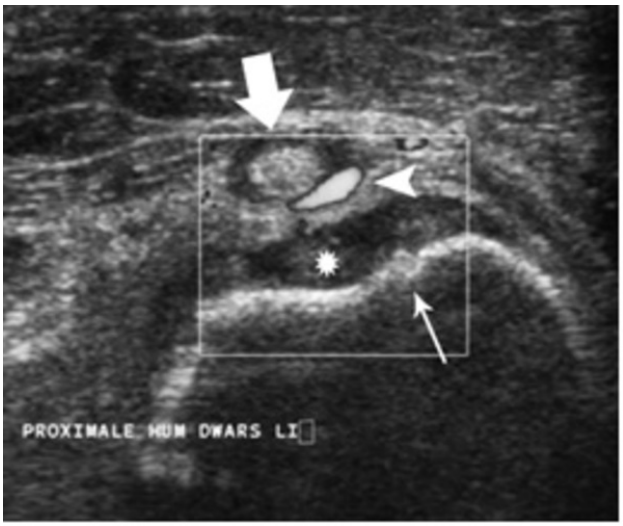

Fig. 11 a

Fig. 11 b

Fig. 11: Acute childhood osteomyelitis of the proximal humerus on ultrasound. Transverse (Fig. 11 a) and longitudinal (Fig. 11 b) ultrasound images. Note focal thinning of the humeral cortex (white arrow) on the axial images in keeping with a cortical penetration of the infection causing subperiosteal pus collection (white asterisk). There is also increased Doppler signal (white arrow head) within the synovium of the biceps tendon (large white arrow).

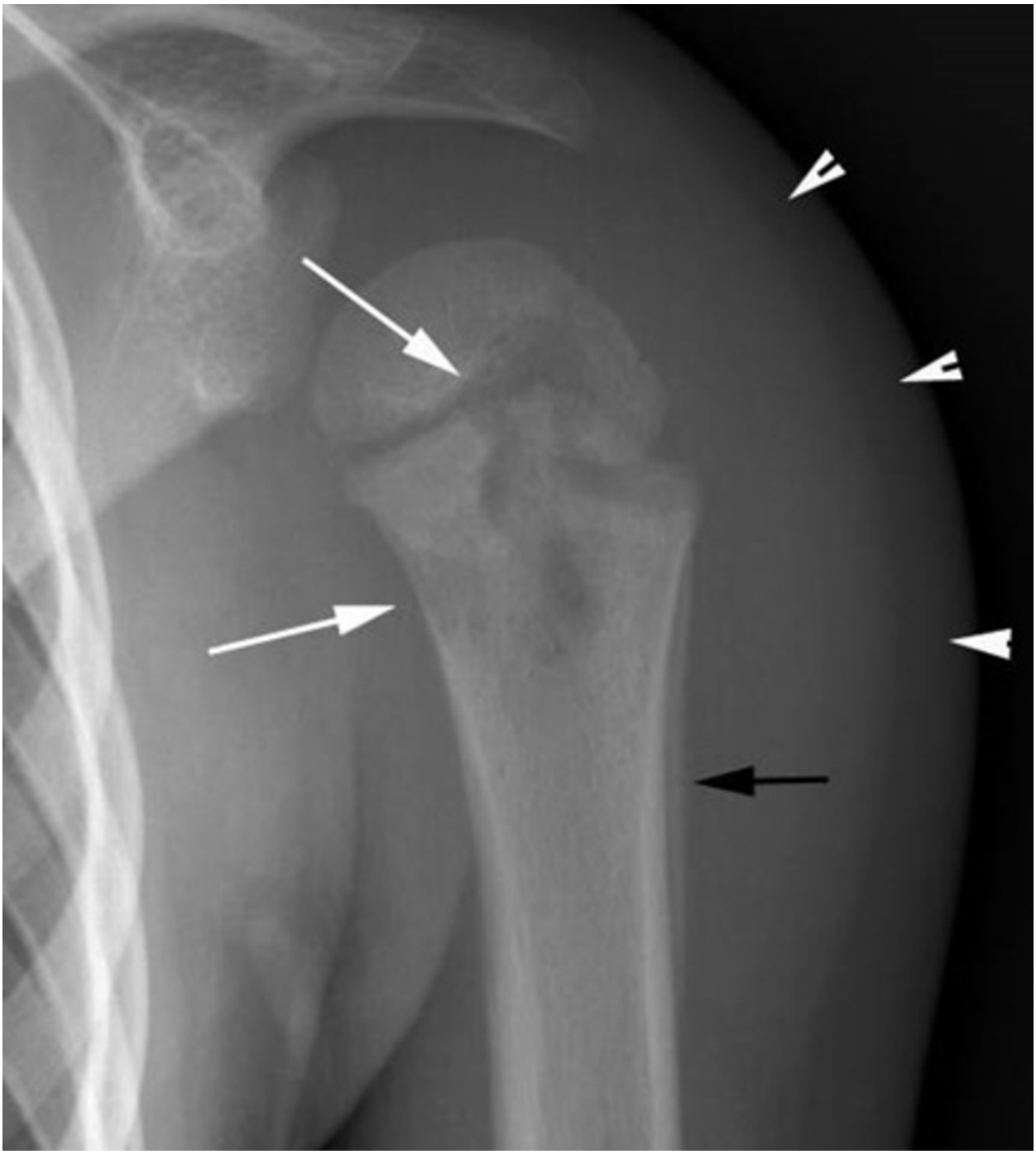

Fig. 12: Acute osteomyelitis of the left humerus. Plain radiography shows an irregularly delineated osteolytic focus within the metaphysis of the humerus (white arrows). Note also periosteal reaction at the proximal humerus diaphysis (black arrow). Associated soft tissue swelling is indicated by the white arrowheads.

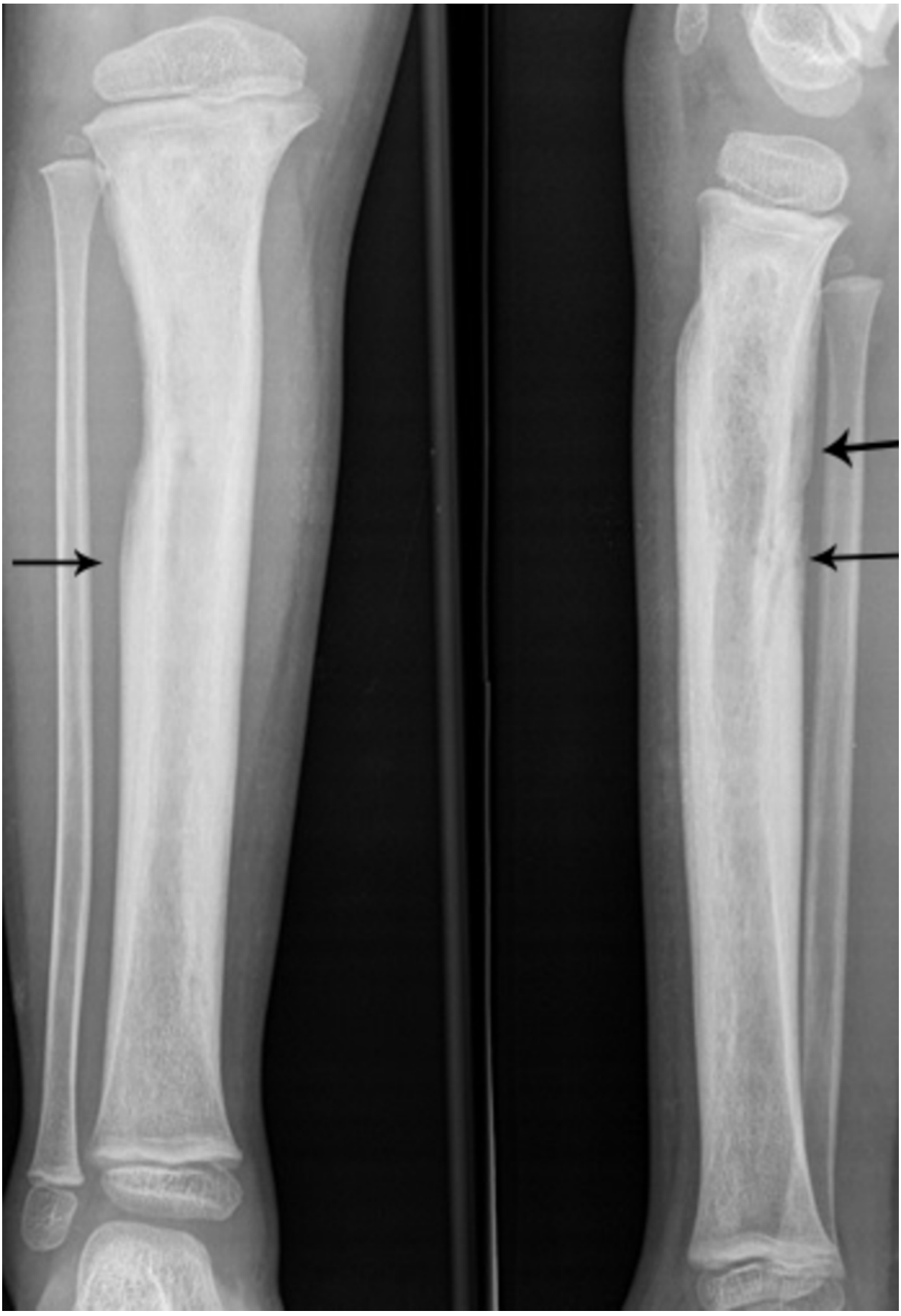

Fig. 13: Extensive involucrum on plain radiography. AP and lateral plain radiography showing extensive involucrum (black arrows) at the tibial diaphysis.

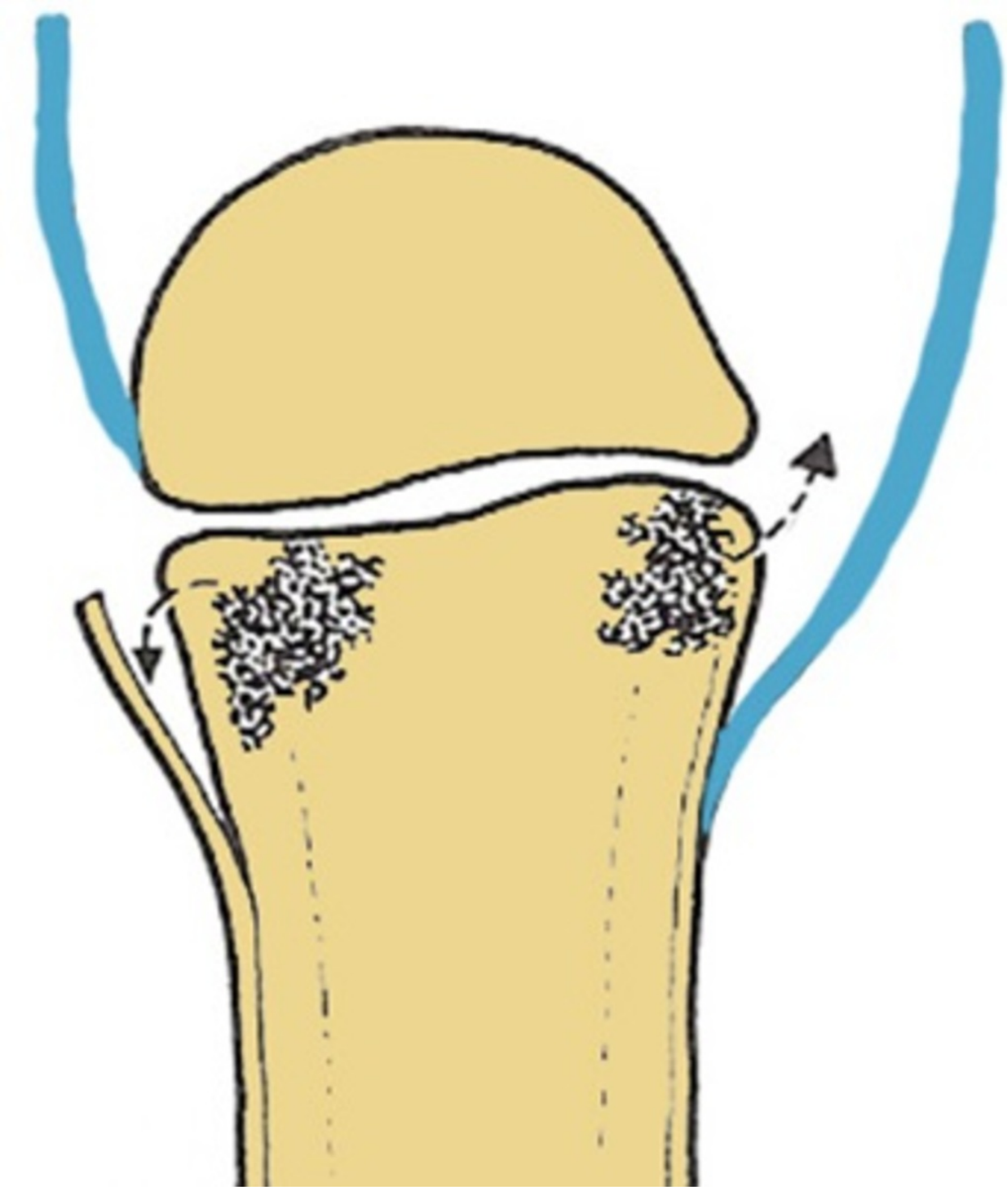

Fig. 14: Schematic drawing of pathogenesis of joint contamination in osteomyelitis. Intra-articular location of the growth plate may lead to rapid spread of infection into the adjacent joint (right side of the drawing). Extra-articular growth plate protects against joint contamination (left side of the drawing).

Fig. 15 a

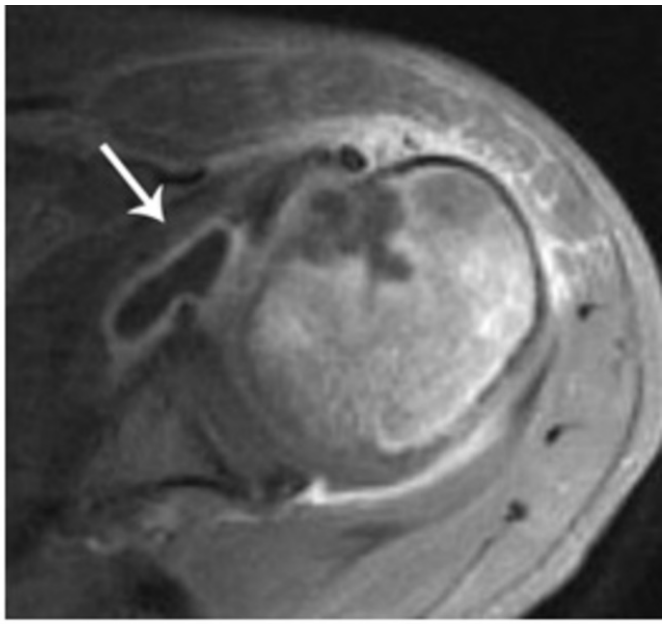

Fig. 15 b

Fig. 15: Joint contamination of acute osteomyelitis of the left shoulder. Coronal (Fig. 15 a) and axial (Fig. 15 b) T1-WI with FS after gadolinium administration. Note the metaphyseal osteomyelitis extending through the medial cortex into the shoulder joint (white arrow).

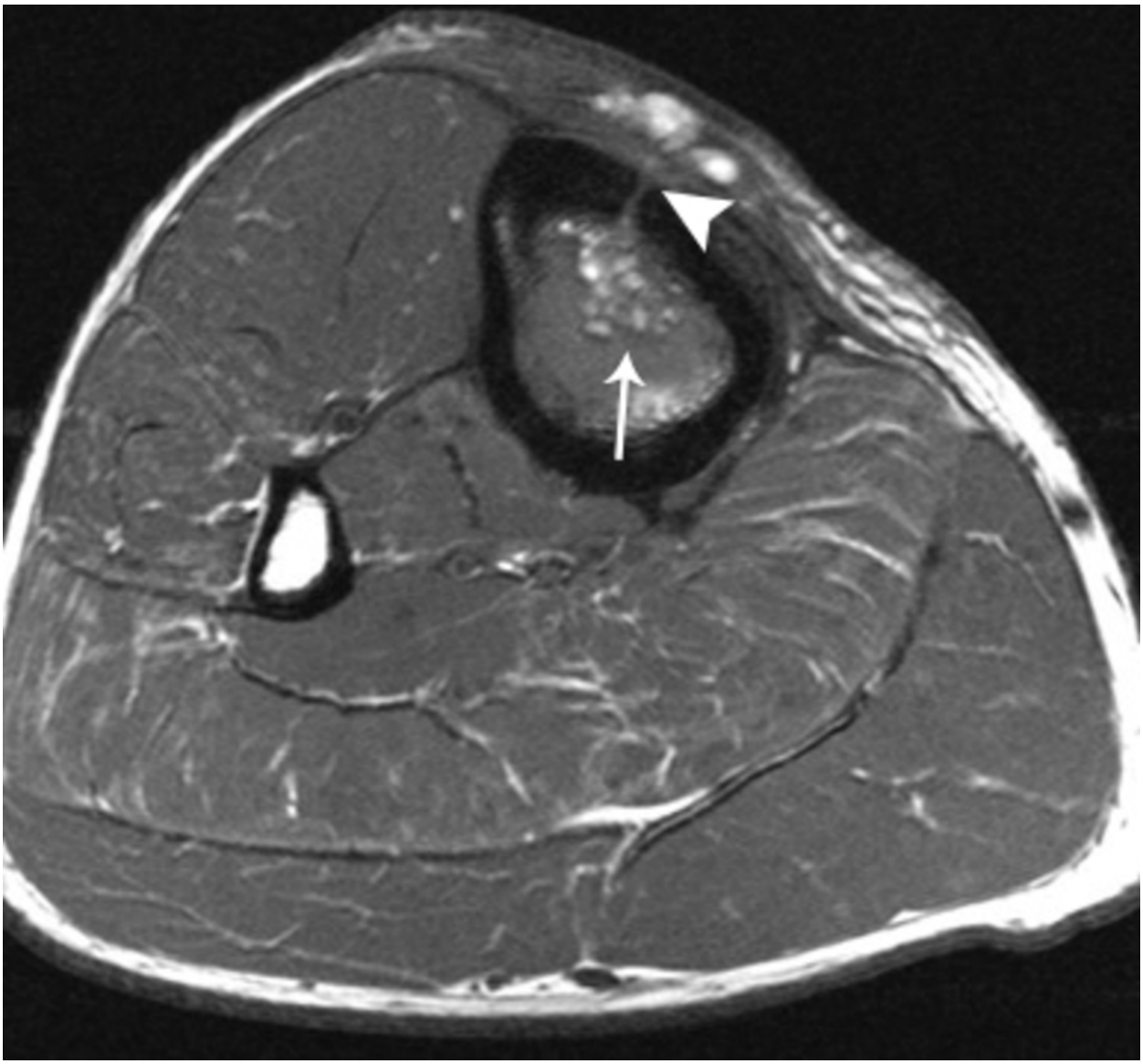

Fig. 16: Fat globule sign on T1-WI. Axial T1-WI showing pathognomonic fat globules (white arrow) within the bone marrow edema of the tibia. In addition a cortical defect perforating the ventral cortex of the tibia or cloaca (white arrowhead) is visualized.

Fig. 17: Typical Brodie abscess in subacute osteomyelitis of the tibia. Lateral plain radiography shows a focal zone of metaphyseal osteolysis with a peripheral rim of reactive sclerosis (black arrows).

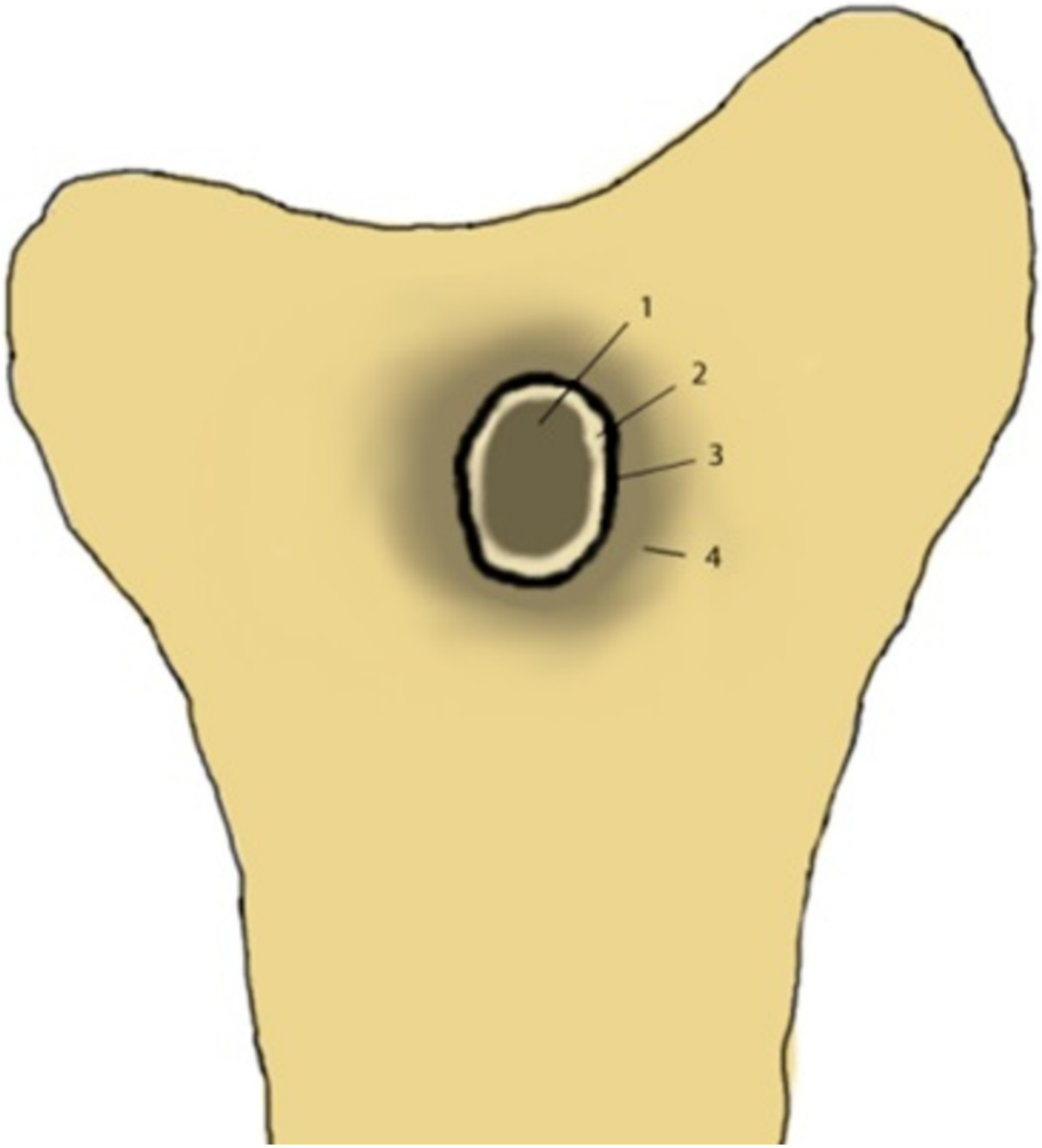

Fig. 18: Schematic drawing of Brodie abscess on T1-WI. 1. Central pus of intermediate to low SI on T1-WI and high SI on T2-WI 2. Internal abscess wall consisting of granulation

tissue of high SI on T1-WI (penumbra) and intermediate SI on T2-WI 3.External ring of reactional sclerosis of low SI on both T1-WI and T2-WI 4.Peripheral bone marrow edema of intermediate to low SI on T1-WI and high SI on T2-WI

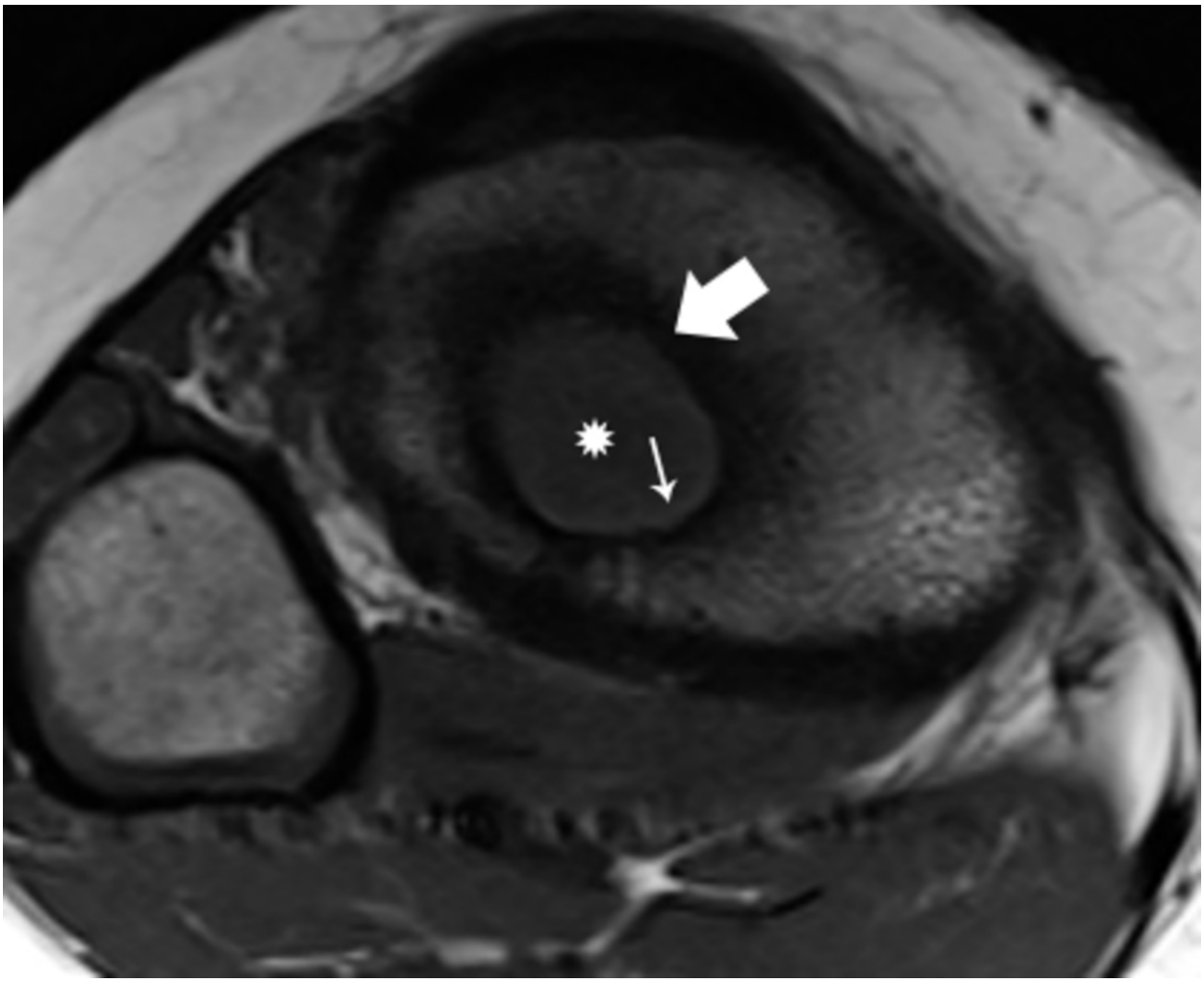

Fig. 19: Penumbra sign on T1-WI. The penumbra sign (small white arrow) is of high signal intensity on this axial T1- WI. The central cavity (white asterisk) is of intermediate to low SI, whereas the peripheral ring of sclerosis is hypo-intense on T1-WI (large white arrow).

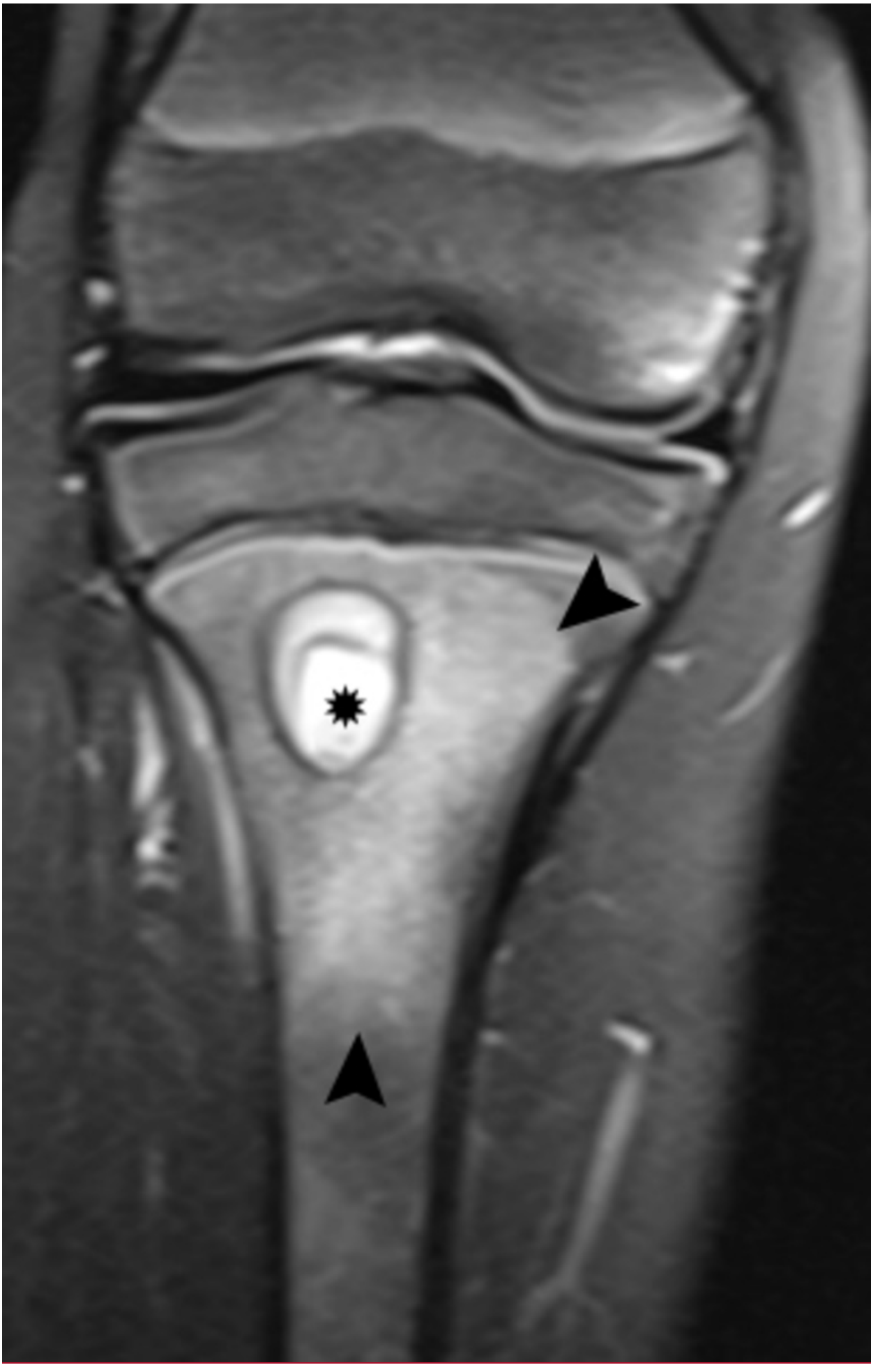

Fig. 20: Brodie abscess in subacute osteomyelitis. Coronal FS T2-WI visualizes the surrounding medullary bone marrow edema (black arrowheads). The central pus collection (black asterisk) of the Brodie abscess has a fluid-like appearance, whereas the periphery is hypointense (corresponding with the sclerotic rim on Fig. 17).

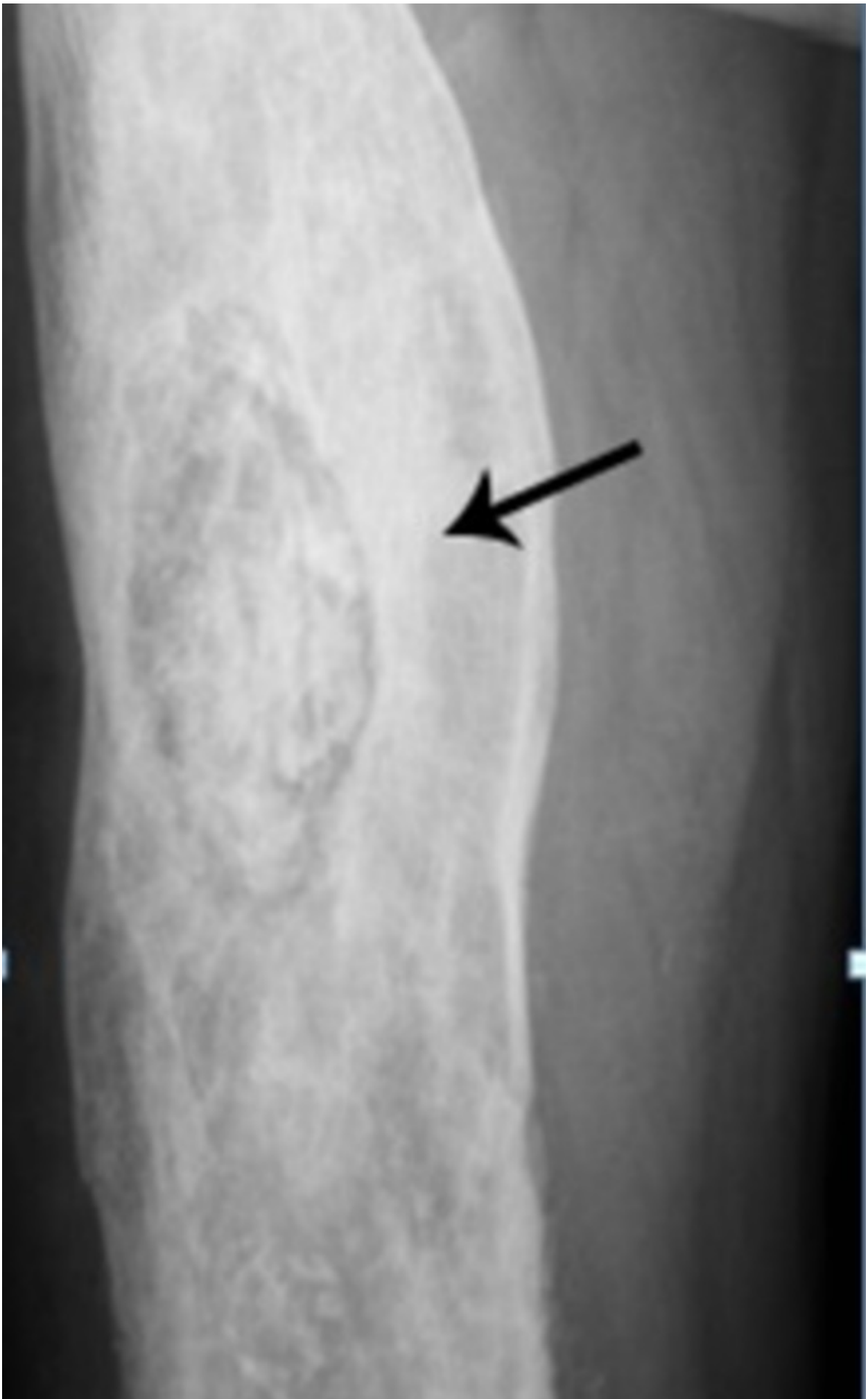

Fig. 21: Chronic osteomyelitis on plain radiography. Plain radiography shows diffuse inhomogeneous osteosclerosis of the right femur. Note the increased density of the bone representing necrotic bone or sequestrum (black arrow).

Fig. 22 a

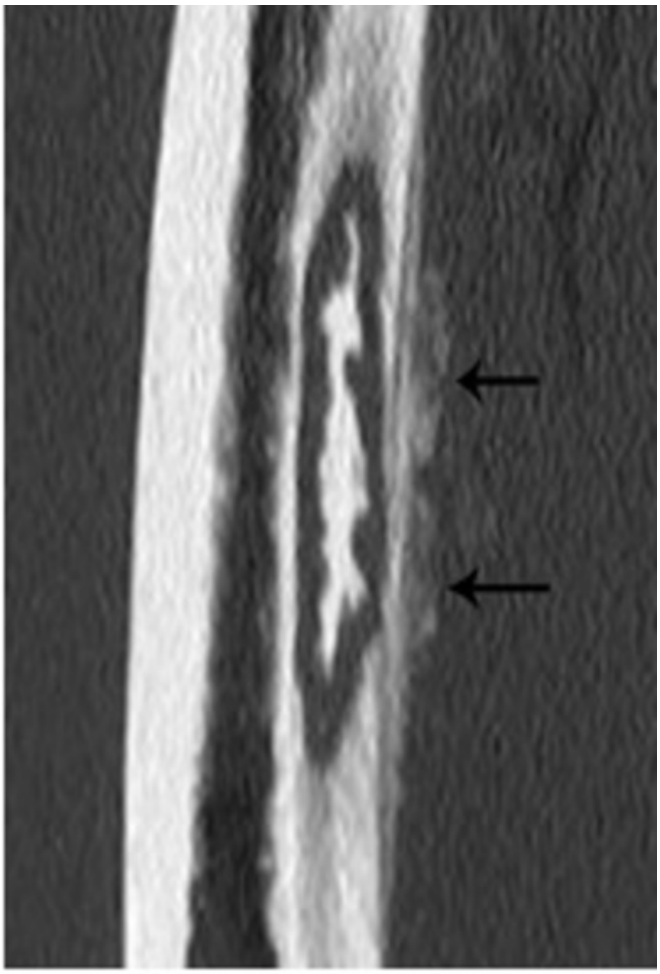

Fig. 22 b

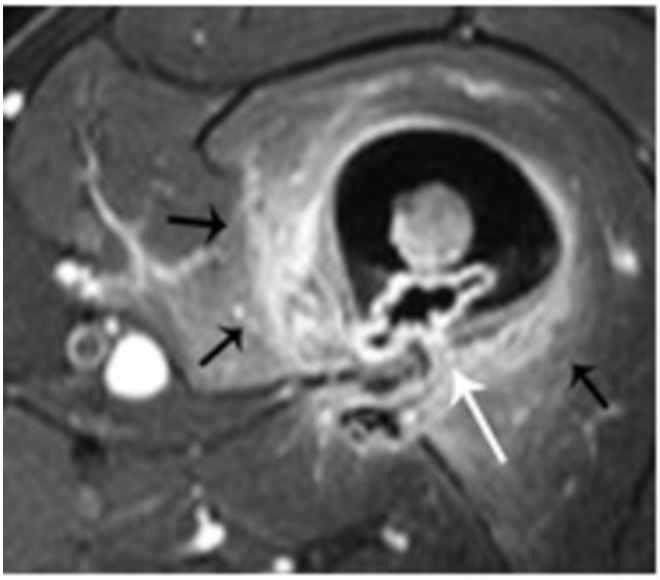

Fig. 22 c

Fig. 22: Chronic osteomyelitis with sequestrum formation. Sequestrum formation with periosteal reaction (arrows) is visualized on plain radiography (Fig. 22 a) as on CT imaging (Fig. 22 b). Axial T1-WI with FS after Gadolinium contrast administration (Fig. 22 c) shows intracortical sequestrum formation (white arrow) of the posterior cortex of the femur with surrounding enhancement of bone marrow and soft tissue (black arrows)(9).

Fig. 23 a

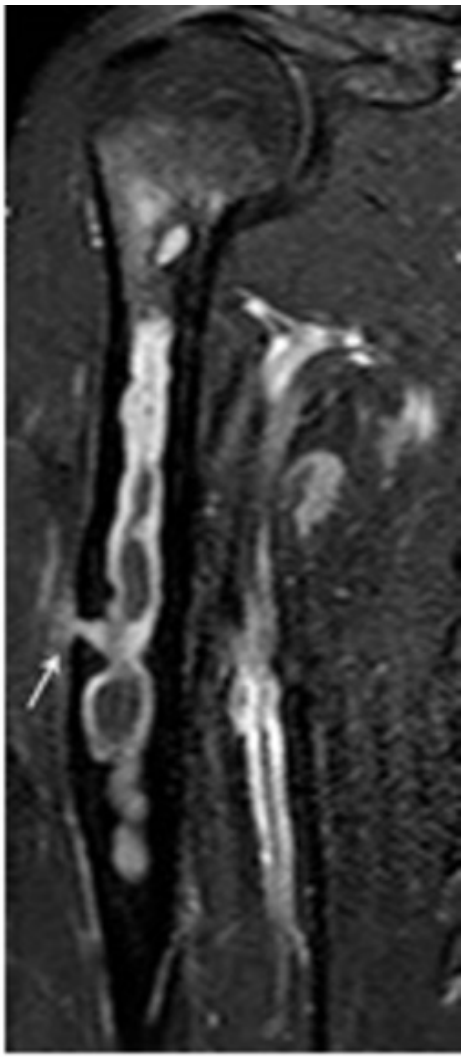

Fig. 23 b

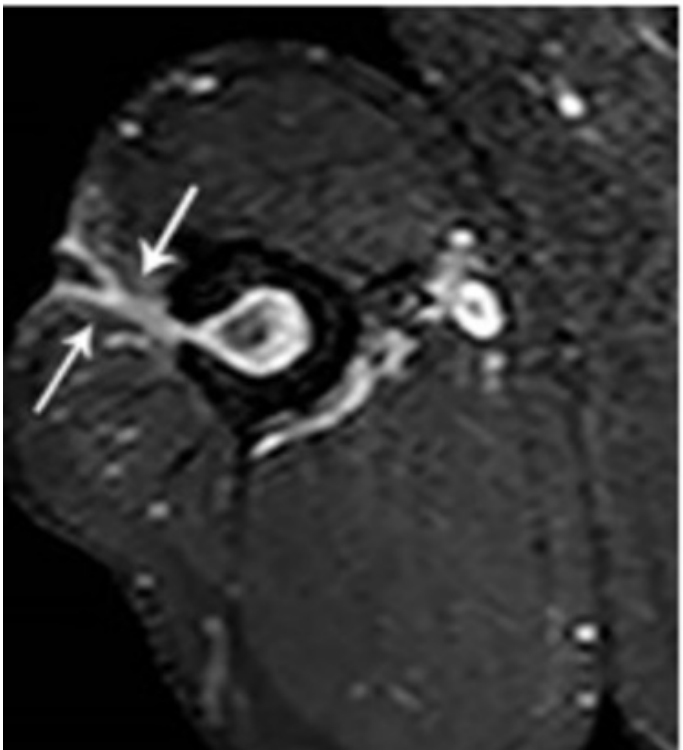

Fig. 23: Chronic osteomyelitis of the right humerus with fistula formation. Plain radiography (fistulography) (Fig. 23 a), coronal (Fig. 23 b) and axial (Fig. 23 c) T1-WI with FS after gadolinium contrast administration. The fistulography (Fig 23 a) shows an intramedullary well defined lytic lesion with scalloping of the cortex. Note the presence of a catheter in the fistula. There is enhancement of the wall of the intra-osseous abscess and the wall of the fistula (white arrows) (Fig 23 b,c). Image courtesy Dr.H. Declercq, Dendermonde

Fig. 24 a

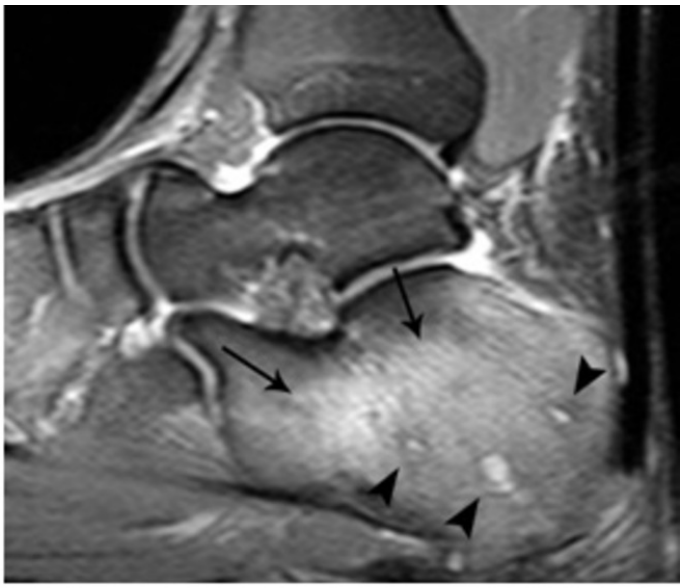

Fig. 24 b

Fig. 24: Chronic osteomyelitis of the calcaneus. Plain radiography (Fig. 24 a) and sagittal FS T2-WI (Fig. 24 b). Plain radiography (Fig. 24 a) shows inhomogeneous sclerosis (black arrows) in the calcaneus. Bone marrow edema is seen on MRI imaging (Fig. 24 b). Note also the presence of small micro-abscesses (black arrowheads).

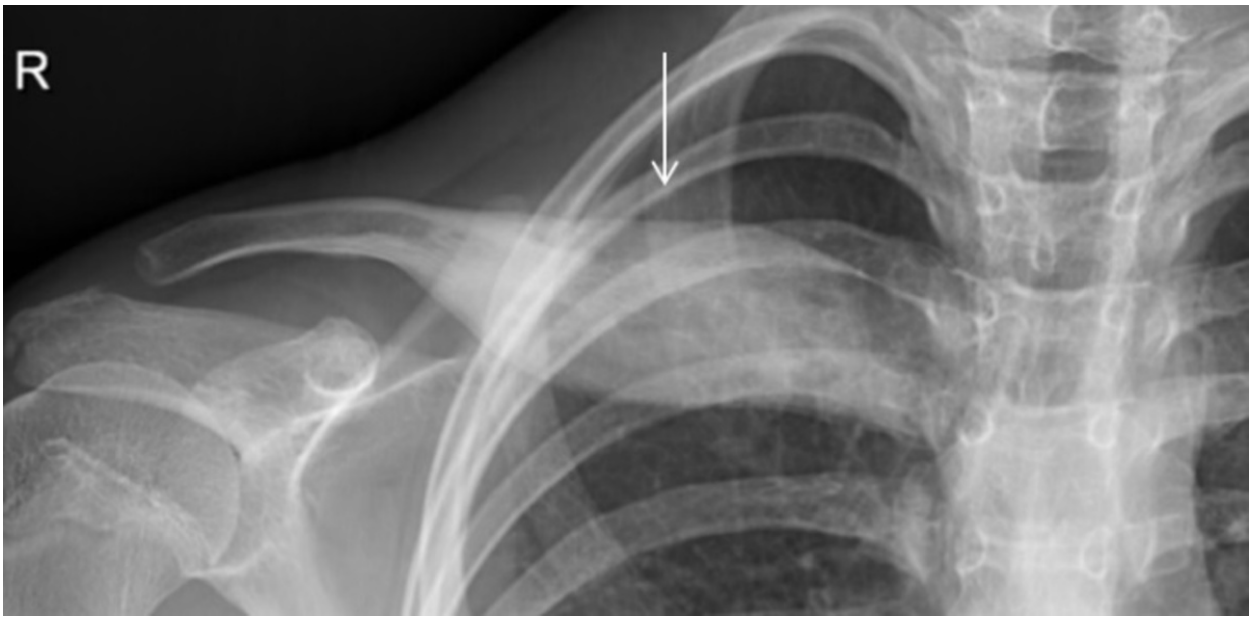

Fig. 25: CRMO of the medial clavicle on plain radiography. Plain radiography shows an expansile lytic lesion (white arrow) of the medial clavicle with extensive bone sclerosis and a solid periosteal reaction.

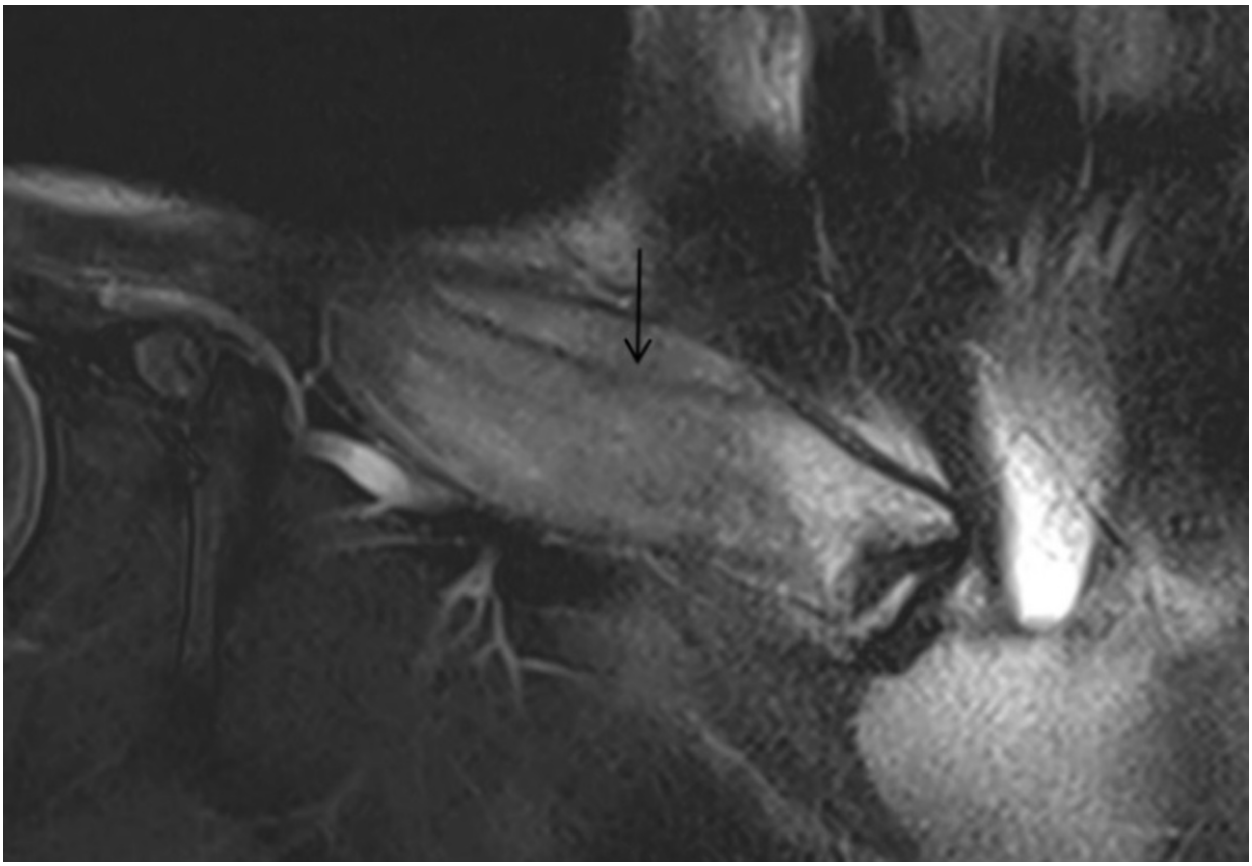

Fig. 26: MRI imaging of CRMO of the medial clavicle in the same patient. Coronal T2-weighted imaging with FS. Note osseous expansion of the lesion beyond the original cortex of the clavicle (black arrow). The lesion has a hypo-intense appearance compared to fluid.

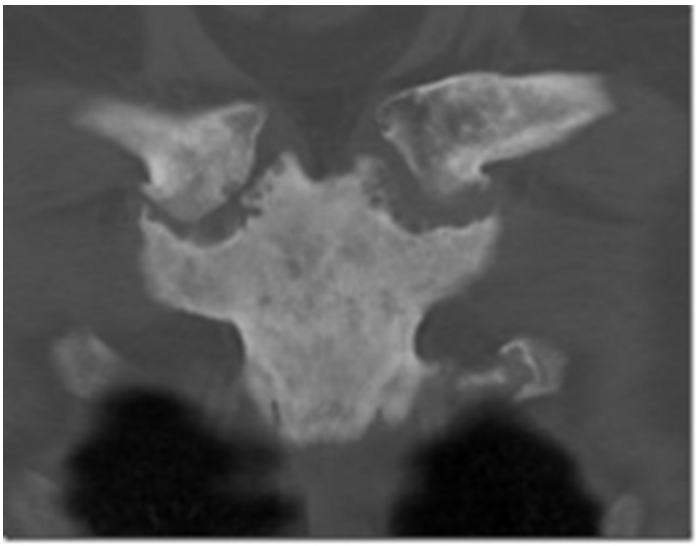

Fig. 27 a

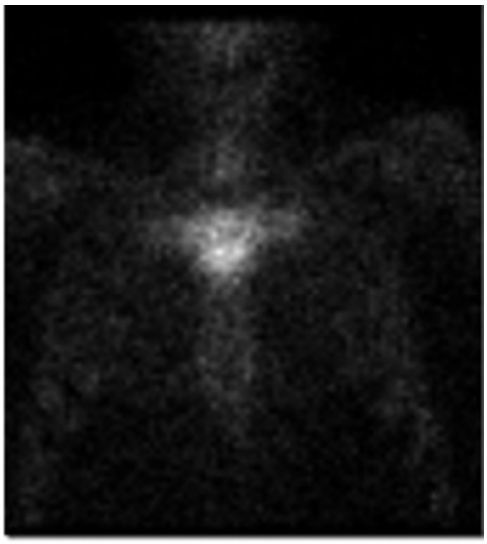

Fig. 27 b

Fig. 27: Typical bullhead sign in SAPHO of the sternoclavicular joint. CT (coronal reformatted image) (Fig. 27 a) shows sclerosis of the manubrium sterni and medial clavicles and erosions of the sternoclavicular joints. Note the typical bullhead sign on the scintigraphy (Fig. 27 b).

Fig. 28: SAPHO of the spine. Sagittal FS T2-WI. Note the hyper-intense bone marrow edema (black arrowheads) in the involved thoracic vertebrae. Paravertebral ossification can be seen (black arrows). Note also prevertebral soft tissue swelling.

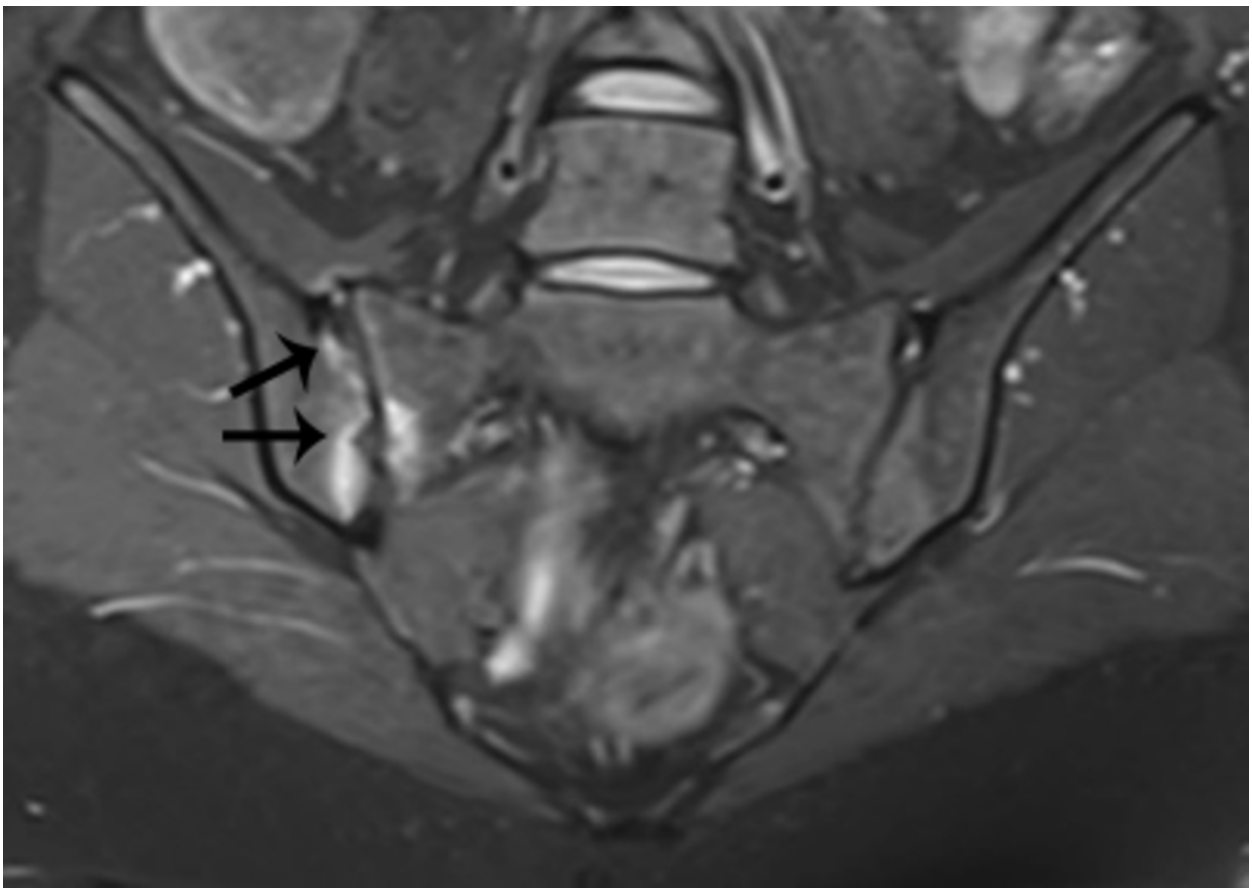

Fig. 29: Early infectious sacroiliitis. FS T2-WI shows marrow edema at the sacral and iliac side of the right SIJ. Note small subchondral erosions (black arrows). Unilateral involvement of the SIJ is very suspicious for infectious sacroiliitis. Often there is rapid destruction of the joint space.

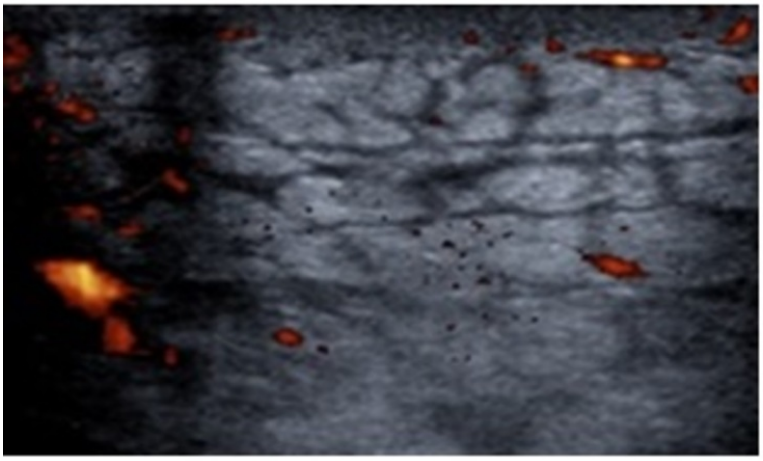

Fig. 30 a

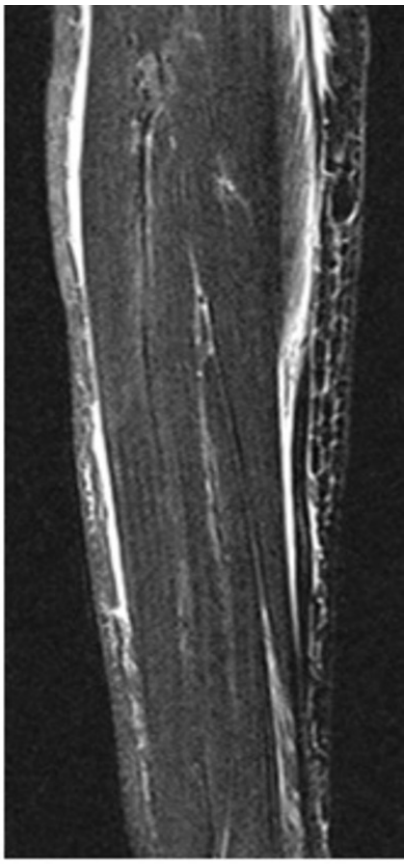

Fig. 30 b

Fig. 30: Cellulitis of the leg. Longitudinal ultrasound (Fig. 30 a) and coronal FS T2-WI (Fig. 30 b. The cellulitis is limited to the superficial fascia. There is pathognomonic cobble stone appearance. Hypervascularity of the subcutis is shown on power Doppler (Fig. 30 a). Note increased signal intensity of the subcutaneous fat on FS T2-MRI imaging (Fig. 30 b).

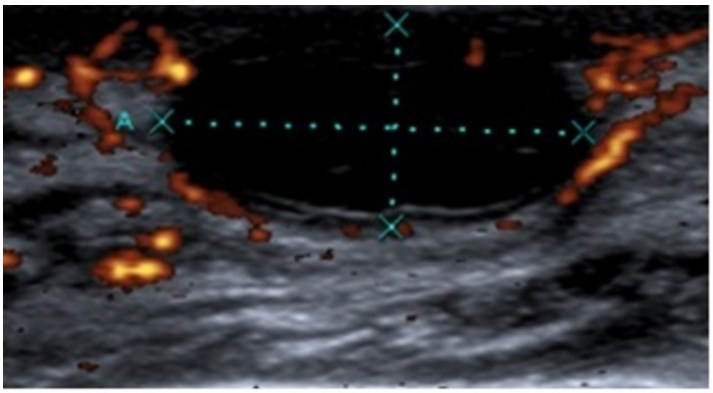

Fig. 31 a

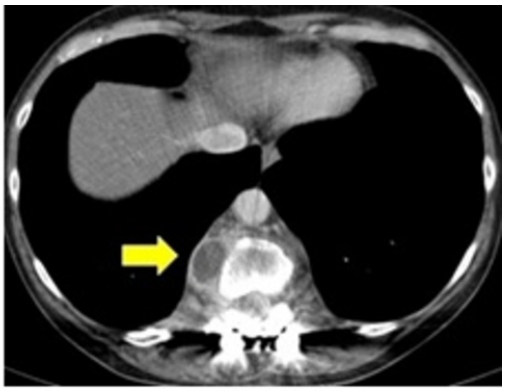

Fig 31. b

Fig. 31: Abscess. Ultrasound imaging (Fig. 31 a) and axial CT (Fig. 31 b). Ultrasound of a subcutaneous abscess shows an anechoic fluid collection with a vascularized pseudocapsule (Fig. 31 a). A paravertebral abscess in another patient showing a central hypodense component and enhancing vascularized capsular ring (yellow arrow). Note also the presence of fusion material in the thoracic spine (Fig. 31 b).

Fig. 32: Post-operative abscess. Post-operative status after left thoracotomy and superior lobectomy. CT imaging shows a subcutaneous abscess containing air bubbles (white arrow) adjacent to the scapula with extent into the left hemithorax. Note multiple enlarged lymph nodes in the left axilla (white arrowhead).

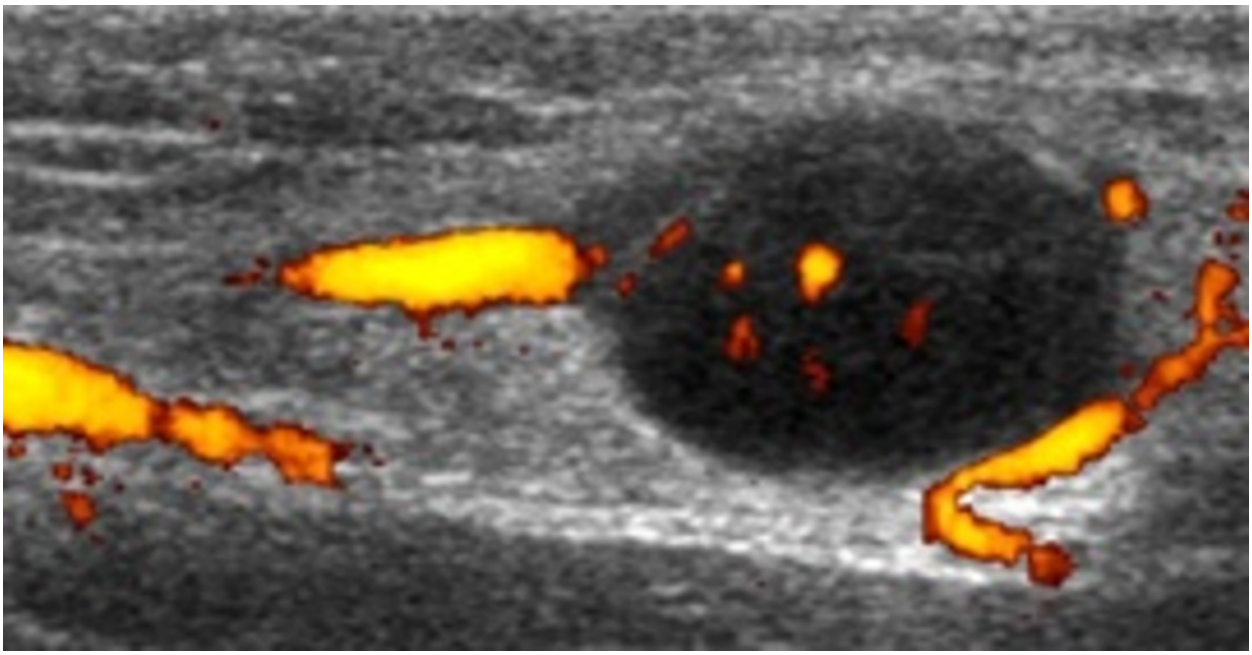

Fig. 33: Cat scratch disease. Ultrasound imaging visualizes lymphadenopathy with intranodal and perinodal hyperemia on power Doppler.

Fig. 34: Frictional bursitis. Longitudinal ultrasound of the shoulder. Extensive fluid in the subacromial-subdeltoid bursa (white arrows) due to repetitive impingement. The supraspinatus muscle is intact.

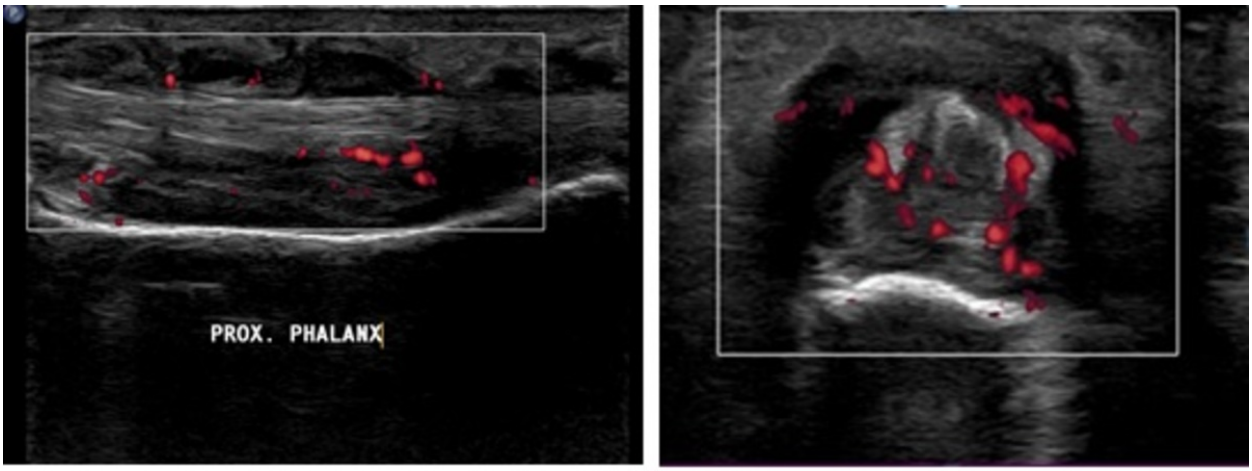

Fig. 35 a

Fig. 35 b

Fig. 35: Infectious tenosynovitis of the flexor tendons of the third finger of a patient working in a slaughterhouse. Longitudinal (Fig. 35 a) and transverse (Fig. 35 b) ultrasound images. Note thickening of the synovium of the flexor tendon of the third finger with an increased power Doppler signal.


R

Fig. 36: Intermediate stage RA. Plain radiography of the right hand showing narrowing of the metacarpophalangeal joints (white arrowheads) and narrowing of the PIP joint of the third and fifth finger (white arrows). Note also cartilage loss at the carpometacarpal joint 1, radiocarpal joint and carpal ankylosis.

Fig. 37: Intermediate stage RA. Plain radiography of the finger showing marginal erosions at the proximal interphalangeal joint (black arrow).

Fig. 38: End stage RA. Plain radiography. Note subluxation of the metacarpophalangeal joint caused by ligamentous involvement.

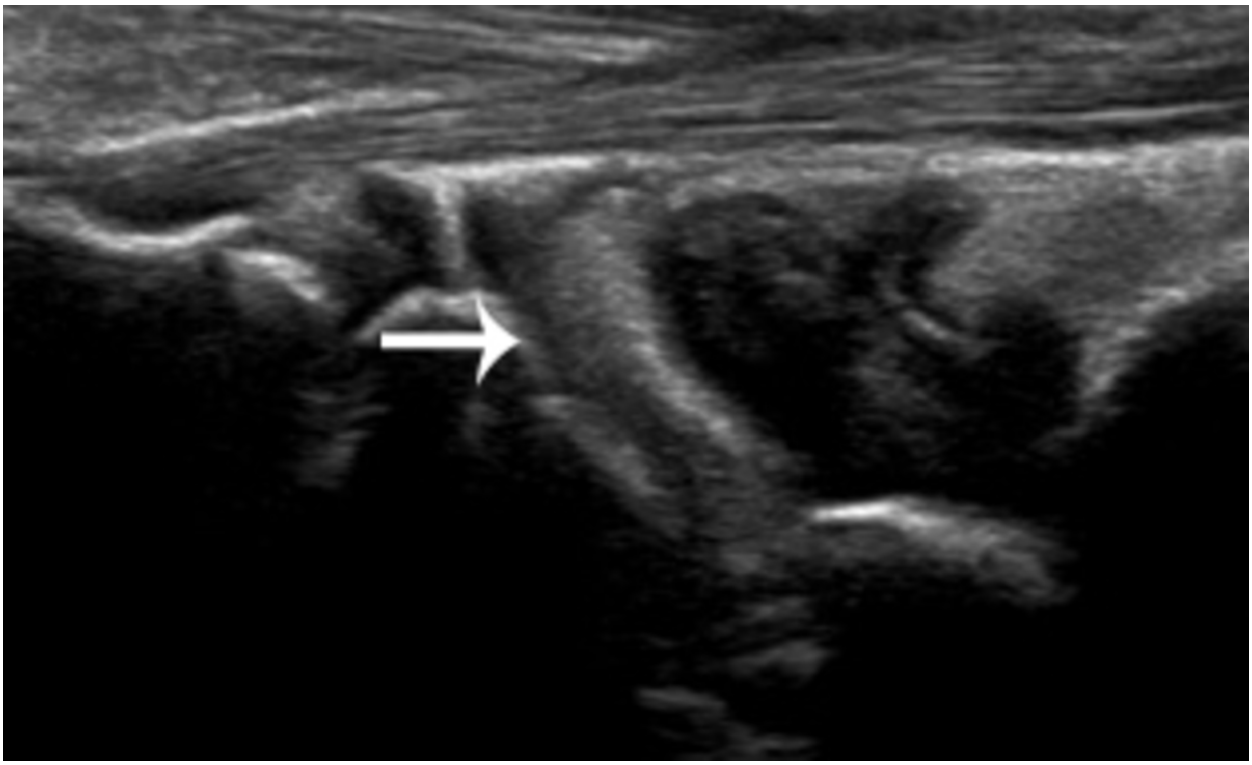

Fig. 39: Synovial pannus on ultrasound. Longitudinal plane ultrasound image showing a hypoechoic edematous thickened synovium (white arrow).

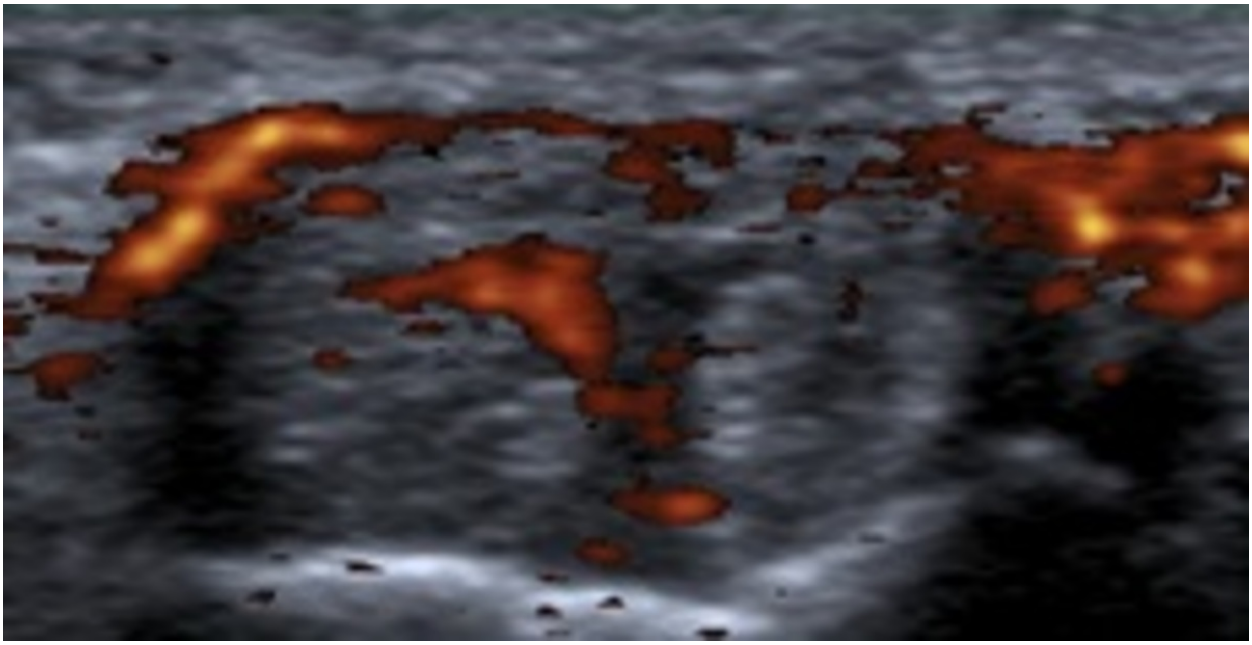

Fig. 40: Synovial inflammation in tendon sheaths. Ultrasound imaging. Axial image. Note the increased Power Doppler signal of the left extensor carpi radialis longus and brevis.

Fig. 41: Intermediate stage RA on MRI. T2-WI. Note the subchondral erosion (white arrow) distal in the proximal phalanx with surrounding bone marrow edema.

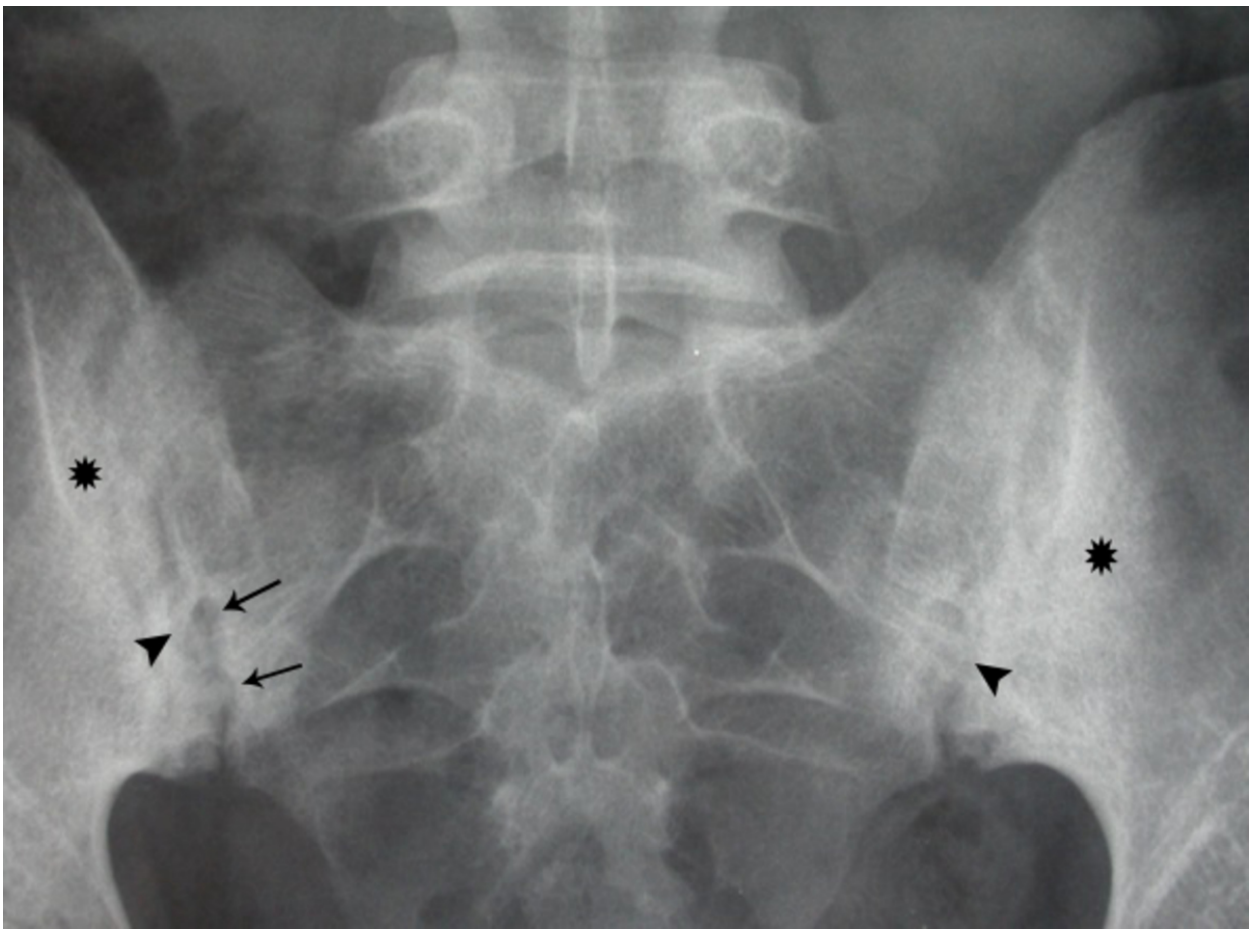

Fig. 42: Variegated sacroiliitis. Plain radiography showing bilateral sacroiliitis with sclerosis (asterisk), widening of the joint space, partial bridging (black arrowheads) and erosions (black arrows) .

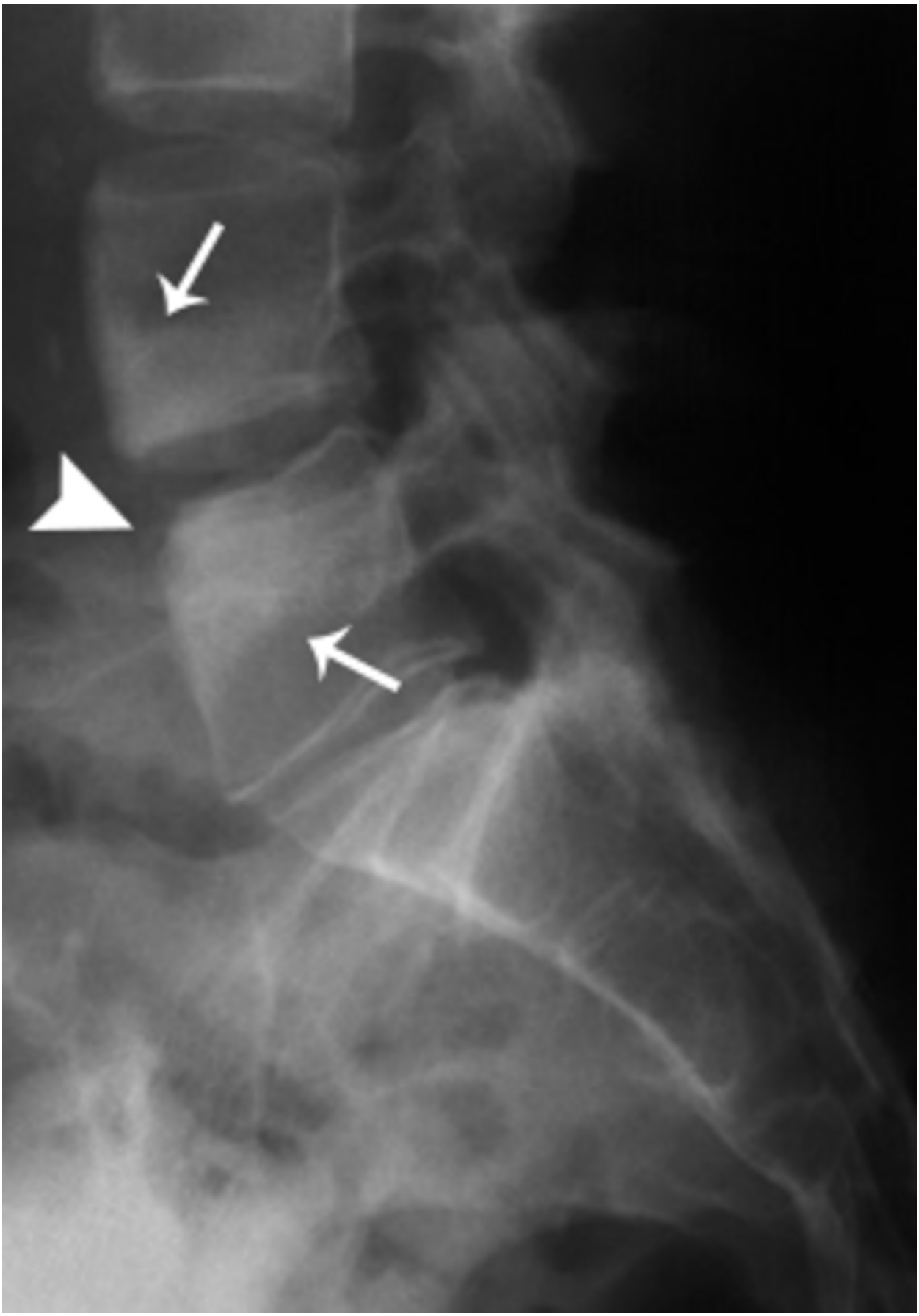

Fig. 43: Shiny corner sign (Romanus lesion) on plain radiography. Shiny corner sign on plain radiography is a late finding of inflammatory spondylarthropathies representing triangular regions of reactive sclerosis (white arrows). There is also erosion of anterosuperior corner of L5 (white arrowhead). Note squaring of the vertebral body L4.

Fig. 44: Early Romanus lesion on MRI. Sagittal T2-WI. Bone marrow edema (white arrow) at the anterosuperior corner of the involved lumbar vertebra in spondylarthropathy. Note subtle underlying erosion of the anteroinferior border of the endplate (white arrowhead).

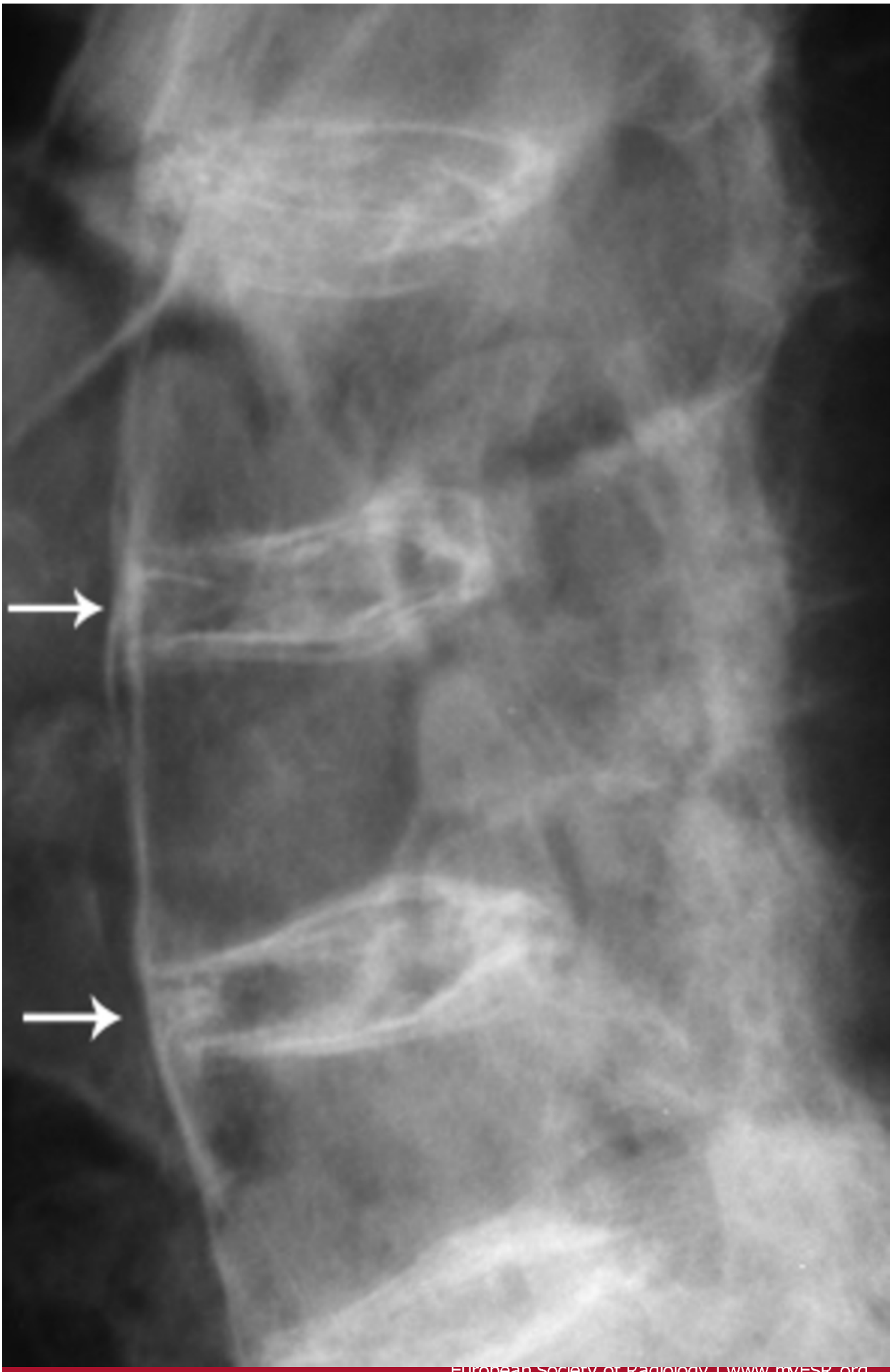

Fig. 45: Bamboo spine due to ankylosis of the spine. Plain radiography of longstanding ankylosing spondylitis. Note the prevertebral ossifications (white arrows) due to ossification of the anterior part of the annulus fibrosus underneath the anterior longitudinal ligament.

Personal information

Julie Desimpel is currently resident in radiology:

- Department of Radiology, AZ Sint-Maarten Duffel-Mechelen, Belgium
- Department of Radiology, Antwerp University Hospital, Antwerp University, Belgium

Magdalena Posadzy is affilated as radiologist to:

- Department of Radiology, W. Dega Orthopaedic and Rehabilitation University Hospital, Karol Marcinkowski University of Medical Sciences, Poznan, Poland

Filip M. Vanhoenacker is affiliated as radiologist to:

- Department of Radiology, AZ Sint-Maarten Duffel-Mechelen, Belgium
- Department of Radiology, Antwerp University Hospital, Faculty of Medicine and Health Sciences, Antwerp University, Belgium
- Faculty of Medicine and Health Sciences, Ghent University, Belgium

References

1. Wessels MI, Baeyaert M, Termote JL, Vanhoenacker FM, De Schepper AM, Parizel PM (2010) Acute osteomyeltitis. JBR-BTR 93:107

2. Hatzenbuehler J, Pulling TJ (2012) Diagnosis and management of osteomyelitis. Insights imaging 3:519-33

3. Pineda C, Espinosa R, Pena A (2009) Radiographic imaging in osteomyelitis: the role of plain radiography, computed tomography, ultrasounds, magnetic resonance imaging and scintigraphy. Radiographic imaging in osteomyelitis 23: 80-9

4. Gold RH, Hawkins RA, Katz RD (1991) Bacterial osteomyelitis: findings on plain radiography, CT,MR, and scintigraphy. AJR 157: 365-70

5. Van Schuppen J, Van Doorn M, Van Rijn RR (2012) Childhood osteomyelitis: imaging characteristics. Insights imaging 3:519-33

6. Smith BJ, Buchanan GS, Shuler FD (2016) A comparison of imaging modalities for the diagnosis of osteomyelitis. Marshall journal of medicine 2(3): 84-92

7. Goossens V, Vanhoenacker FM, Samson I, Brys P (2010) Longitudinal cortical split sign as a potential diagnostic feature for cortical osteitis. JBR-BTR 93(2):77-80

8. Goossens V, Vanhoenacker FM, Samson I, Brys P (2010) Longitudinal cortical split sign as a potential diagnostic feature for cortical osteitis. JBR-BTR 93(2):77-80

9. Davies AM, Grimer R (2005) The penumbra sign in subacute osteomyelitis. Eur radiol 15:1268-70

10. Goossens V, Vanhoenacker FM, Samson I, Brys P (2010) Longitudinal cortical split sign as a potential diagnostic feature for cortical osteitis. JBR-BTR 93(2):77-80

11. Desimpel J, Vanhoenacker FM (2017) Chronic recurrent multifocal osteomyelitis (CRMO) of the clavicle. Eurorad 10.1594/EURORAD/CASE.14212

12. Rahmouni A, Chosidow O, Mathieu D et al. (1994) MR imaging in acute infectious cellulitis. Radiology 192(2): 493-6

13. Hayeri MRH, Ziai P, Shehata ML, Teytelboym OM, Huang BK (2016) Soft-tissue infections and their imaging mimics: from cellulitis to necrotizing fasciitis. RadioGraphics 36:1888-1910

14. Schmid MR, Kossmann T, Duewell S (1998) Differentiation of necrotizing fasciitis and cellulitis using MRI imaging. AJR 170(3):615-20

15. Geata M, Mazziotti S, Minutoli F, Genitori A, Toscano A, Rodolico C, Blandino A (2008) MR imaging findings of focal myositis: a pseudotumor that may mimic muscle neoplasm. Skeletal Radiol 38:571-8

16. Gaspari R, Dayno M, Briones J, Blehar D (2012) Comparison of computerized tomography and ultrasound for diagnosing soft tissue abscesses. Critical Ultrasound Journal 4(1): 1-7

17. Melville DM, Jacobson JA, Downie B, Biermann JS, Kim SM, Yablon CM (2015)Sonography of cat scratch disease. J Ultrasound Med 34(3): 387-94

18. Hopkins KL, Simoneaux SF, Patrick LE, Wyly JB, Dalton MJ, Snitzer JA (1996) Imaging manifestations of cat-scratch disease. AJR 166: 435-8

19. Dong PR, Seeger LL, Panosian CB, Johnson BL, Eckardt JJ (1995) Uncomplicated cat-scratch disease: findings at CT, MR imaging, and radiography. Radiology 195(3): 837-9

20. Floemer F, Morrison WB, Bongartz G, LedermannHP (2004) MRI characteristics of olecranon bursitis. AJR 183: 29-34

21. Patil P, Dasgupta B (2012) Role of diagnostic ultrasound in the assessment of musculoskeletal diseases. Ther Adv Musculoskelet Dis 4(5): 341-55

22. Sommer OJ, Kladosek A, Weiler V et al. (2005) Rheumatoid arthritis: a practical guide to state-of-the-art imaging, image interpretation, and clinical implications. Radiographics. 25 (2): 381-98

23. Sommer OJ, Kladosek A, Weiler V, Czembirek H, Boeck A, Stiskal M (2005) Rheumatoid Arthritis: a practical guide to state-of-the-art imaging, image interpretation and clinical implications. RadioGraphics 25:381-98

24. Lambrecht V, Vanhoenacker FM, Van Dyck P, Gielen J, Parizel PM (2005) Ankylosing spondylitis: what remains of the standard radiography anno 2004? JBR-BTR 88(1) 25-30

25. Hermann KGA, Althoff CE, Schneider U, Zühlsdorf S Lembcke A, Hamm B, Bollow M (2005) Spinal changes in patients with spondyloarthritis: comparison of MR imaging and radiographic appearances. RadioGraphics 25:559-70

26. Vanhoenacker FM, Eyselbergs M, Cotten A (2011) Spinal degeneration: beyond degenerative disc disease: how to discriminate degeneration from spondylarthropathies? Neuroradiology 53(1): 175-9

27. Navallas M, Ares J, Beltran B, Lisbona MP, Maymo J, Solano A (2013) Sacroiliitis associated with axial spondyloarthropathy: new concepts and latest trends. RadioGraphics 33: 933-56

28. Sudol-Szopinska I, Kwiatkowska B, Wlodkowska-Korytkowkska M, Matuszewska G, Grochowska E (2015) Diagnostics of sacroiliitis according to ASAS criteria: a comparative evaluation of convention radiographs and MRI in patients with a clinical suspicion of spondoarthropathy. Preliminary results. Pol J Radiol. 80: 266-76